PHOTOPOLYMERS FOR USE AS HOLOGRAPHIC MEDIA

[1]Michael R. Gleeson

[1]National University of Ireland Maynooth,
Department of Computer Science,
Faculty of Science and Engineering,
Maynooth, Co. Kildare, Republic of Ireland.

[2]Jinxin Guo and [2]John T. Sheridan

[2]UCD School of Electrical, Electronic and Communications Engineering,
College of Engineering, Mathematical and Physical Sciences,
Communications and Optoelectronic Research Centre,
SFI Strategic Research Centre in Solar Energy Conversion,
University College Dublin, Belfield, Dublin 4, Republic of Ireland.

Contact authors: michael.gleeson@ucd.ie, jinxin.guo@ucd.ie, john.sheridan@ucd.ie

ABSTRACT

In this chapter we briefly review some of the developments which have been made in the area of photopolymer material development for applications such as holography. We also examine some of the extensions which have been made to the theoretical models of the processes which occur during free radical photo-polymerisation, namely the Non-local Photo-polymerisation Driven Diffusion (NPDD) model. An understanding of these photochemical and photo-physical processes is of extreme importance when attempting to improve a photopolymer material's performance for a given application. We will explore the most recent developments made and illustrate some of the useful trends, which this NPDD model predicts and then analyze their implications on photopolymer improvement. Among the effects examined are; the temporal and spatial primary radical generation (the driving force of photo-polymerisation), multiple termination mechanisms, non-local polymer chain growth, the effects of oxygen inhibition, mass transport effects (diffusion), dark reactions (post exposure effects) and chain transfer, to name a few.

Keywords: Holography, holographic recording material, photopolymer, chain transfer agent, inhibition, dark reactions, non-local.

1. INTRODUCTION

Photopolymers were first introduced as a holographic recording material by Close *et al*. in 1969, [1]. Since then numerous systems have been examined, but only a small number have become commercially available, [2]. Polymer materials have several advantages. Because thick layers can be fabricated they act as true volume materials giving high diffraction efficiency and good angular selectivity. Most of the materials are self–developing or require only some simple post–processing, such as an exposure to light or heat treatment. This eliminates the need for wet chemical development, which makes photopolymers suitable for applications such as holographic embedded photopolymer waveguides, [3-6] and holographic data storage [7-18].

Photopolymers generally consist of a monomer, a photosensitive dye and an initiator. They can either be liquid or dry layer systems. The dry photopolymers usually contain a polymeric binder in addition to the other components. As mentioned above the first photopolymer material used for holographic recording, was reported by Close *et al*. [1]. This liquid state material consisted of a mixture of acrylamide and metal acrylate monomers and a photocatalyst methylene blue. Sadlej and Smolinska [19] improved the original system proposed by Close by including a poly-vinylalcohol (PVA) binder which allowed the production of dry photopolymer layers.

In the eighties, Calixto [20] continued the work on acrylamide-based systems. The material contained acrylamide monomer, TEA as an electron donor, methylene blue photosensitizer and PVA as a binder. Blaya *et al*., [21], improved the sensitivity of the acrylamide material for recording at 633 nm by changing the crosslinker, *N,N*-dihydroethylenebisacrylamide. A hybrid material containing acrylamide and acrylic acid as monomers was proposed by Zhao *et al*., [22]. The material uses methylene blue as the photosensitizer, TEA and p-toluenesulfonic acid as sensitizers and gelatin as a binder.

While acrylamide based free-radical systems have received much attention in the literature other materials offer advantages when it comes to the development of practical storage media. Trentler *et al*., [23] developed an epoxy resin photopolymer material with a solid matrix, which is formed in situ as the epoxy cures at room temperature. The unreacted vinyl monomers within the material are subsequently photo-polymerized during hologram recording. One of the key features of this type of material is the separation of the epoxy and vinyl polymerizations. This separation allows for a large index contrast to be developed in holograms when components are optimized. This material is functional in thick formats (several millimetres), which enables narrow angular bandwidth and high diffraction efficiency. A dynamic range (M/#) up to 13 has been measured in these materials.

More recently, works have been carried out on the development of a commercial grade acrylate photopolymer with the same two step polymerisation [24], offering very fast response of the refractive index modulation with respect to the recording dosage, particularly at lower power densities, very high storage resolution, and very large refractive index modulation [25,26].

Extensive work has been carried out, in both industry and academia, on the development of these photopolymer materials and more recently on the understanding of the photochemical kinetics associated with them. In order to maximise the potential of these materials for various applications, the necessity for a physically comprehensive theoretical model of the effects which occur during photo-polymerization is becoming ever more important. Providing such a model will enable potential trends in a material's performance to be recognized and optimised, [27]. Such models allow simulations of ratios of various key material components to be made, yielding indications of the most suitable material compositions in order to improve material performance.

In this chapter we examine some recently published results on the Non-local Photo-polymerization Driven Diffusion (NPDD) model, [26-32]. This model provides a comprehensive theoretical representation of the processes, which occur during free radical photo-polymerization. The physically realistic model enables predictions to be made about a number of very different photopolymer materials [26-32]. We present several extensions to the previous model in particular allowing for spatially and temporally varying primary radical generation, oxygen inhibition, dark reactions and chain transfer effects. We then apply this model to analyse a number of effects observed to take place during holographic grating formation in an acrylamide/polyvinylalcohol (AA/PVA) based photopolymer and compare experimental results and the predictions of the model with the aim of characterising these effects.

The chapter is structured as follows: In Section 2 we will briefly examine some of the methods used to measure and monitor the optical performance of holographic gratings in photopolymers. In Section 3 we briefly describe the fundamental photo-kinetic processes, which occur in photopolymers during holographic exposure. Then based on these photo-kinetic processes we construct a set of first order coupled differential equations which represent the temporal and spatial variation of the concentrations of constituents of the photopolymer, which form the basis of the Non-local Photo-polymerization Driven Diffusion (NPDD) model. We then analyse some of the simulated behaviour of this model under given physical conditions to examine its physicality and present some of the predictions made which offer potential methods to improve a photopolymers holographic performance. Following these predictions, in Section 4 we then attempt to improve an acrylamide/polyvinylalcohol (AA/PVA) based photopolymer's spatial frequency response which will increase its high density storage resolution. In Section 5 a brief conclusion is presented offering potential direction for future advancements in the area of photopolymer development.

2. OPTICAL TESTING OF PHOTOPOLYMERS FOR HOLOGRAPHY

In the study of holographic recording materials it is common to record gratings in photosensitive materials, such as photopolymers, and to then optically examine the resulting gratings. The gratings produced are often electromagnetically modelled using Kogelnik's two-wave coupled wave theory. Kogelnik's two-wave coupled wave theory, [35], describes the efficiency with which thick holograms can diffract incident light. Analytic expressions for both the angular and wavelength dependence of the diffraction efficiency as the incident light deviates from the Bragg condition are derived. Thus the dependence of the diffraction efficiency, $\eta(t)$, on a number of grating parameters is known. For a lossless, unslanted transmission geometry grating, replayed on-Bragg with TE polarized probe light, it is shown, [35], that $\eta(t)$ is described by the following equation:

$$\eta(t) = \frac{I_D(t)}{I_{in}} = \sin^2\left[\frac{\pi n_1(t)d}{\lambda\cos\theta}\right],$$

(1)

where I_{in} and $I_D(t)$ are the incident and diffracted probe beam intensities respectively, d represents grating thickness, θ and λ are the Bragg angle and wavelength of incident probe beam inside the grating, and $n_1(t)$ is the refractive index modulation. In deriving Eq (1) all boundary reflections have been neglected.

Rearranging Eq (1) enables an expression for the temporally varying refractive index modulation, $n_1(t)$, to be obtained,

$$n_1(t) = \frac{\lambda\cos\theta}{\pi d}\sin^{-1}\left[\sqrt{\eta(t)}\right].$$

(2)

By monitoring the amount of light diffracted from a weak probe beam during exposure, $I_D(t)$, growth curves of refractive index modulation against exposure time can be extracted. In the majority of the literature, such growth curves are used to monitor grating formation. A typical experimental set-up used to record and monitor these growth curves is presented in Figure 1.

During the grating recording process the evolution of the grating is monitored in real time. One of the main advantages of many photopolymer materials is that they are self-processing and thus, non-latent, [36], therefore the diffractive scattering properties are immediately available as the grating is being formed. This allows the evolution of the grating to be monitored by replaying the grating as it is being recorded using a probe laser with a wavelength, which lies outside the absorption spectrum of the photosensitizer used. This ensures that the probing does not affect the fabrication process. In the set-up presented in Figure 1 the probe laser is operating at $\lambda = 475$ nm, i.e. outside the absorption spectrum of the photosensitizer.
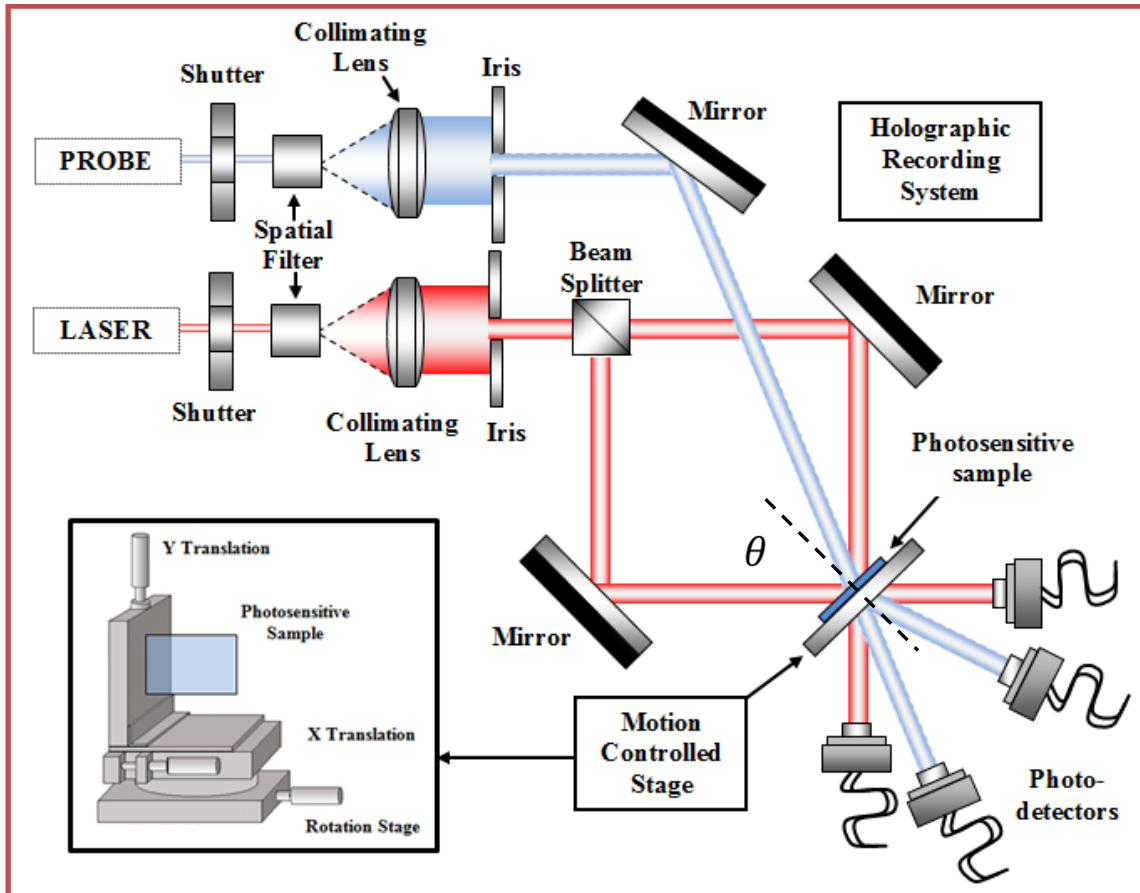
Figure 1. Typical experimental set-up used to record unlsanted volume transmission holographic gratings with a recording wavelength of $\lambda = 633$ nm.

Examining Eq (1) it is clear that the on-Bragg replay angle of the probe beam, θ_r, will be different from the recording angle, θ, due to the variation in the wavelength used, for example $\lambda_{Record} = 633$ nm, $\lambda_{Replay} = 475$ nm. Thus recreation of the object wave, as illustrated in Figure 1, occurs at a different angle due to the change in wavelength. The intensity of the resulting probe diffracted beam, $I_D(t)$, and therefore the diffraction efficiency, will depend on the strength of the grating, i.e. the refractive index modulation, $n_1(t)$. Thus, it is possible to monitor the grating formation (growth curve) by recording the intensity of the diffracted beam as suggested by Eq (1) and Eq (2).

In the above we have emphasised the recording of a single unslanted gratings and the capture of growth curves. However, the photosensitive sample can also be mounted on a rotation and translation stage (as shown in the inset of Figure 1), enabling the analysis of the angular response of the grating and the recording of grating arrays, [37]. In Holographic Data Storage (HDS) where the storage of multiple pages of information is required, these holograms (gratings) are angularly multiplexed on top of each other within the same volume of the holographic medium. It is the ability to achieve this which makes photopolymer materails an attractive media for optical storage.

It must also be noted that using this optical setup, the temporal variation in the absorbance of the photo-sensitiser can be examined. As the recording beams which are used to record the grating, transmit through the photopolymer sample, they can be collected in the photo-detectors shown in Figure 1. Thus enabling key material parameters related to the photo-absorption kinetics and sensitivity of the photopolymer, to be examined.

In the next section we will examine the photo-kinetic and photo-physical behaviour of these photopolymer materials. It is these reactions which are the basis of the theoretical models which are used as photopolymer material optimisation tools and are the fundamental building blocks of the Non-local Photo-polymerisation Driven Diffusion (NPDD) model [11,26-34].

3. PHOTO-KINETIC BEHAVIOUR

Let us begin this section with a review of the kinetic models of photopolymerisation which have been presented in the literature.

3.1 Review of kinetic models

The photochemical processes, which are present during photopolymerization, are complex [11,26-34,38-43], however an understanding of these processes is of utmost importance if a practical model is to be developed. In a recent review, [44] many of the assumptions made in developing photochemical models of free radical photo-polymerisation were discussed, [38-43]. A number of physical effects not included in the current models were listed, which indicated a lack of physicality under certain exposure conditions. Following the appearance of this review, a series of papers were published [30-32] which addressed many of these issues and provided a model containing a consistent set of chemical reaction equations to take into account many of these effects. These effects included;

    i)   Removal of the steady state approximation for macroradical concentration,

    ii)   inclusion of spatially and temporally non-local polymer chain growth,

    iii)   inclusion of time varying photon absorption,

    iv)   simultaneously including the effects of both primary, i.e. $R^{\bullet}$-$M^{\bullet}$, and bimolecular, i.e. $M^{\bullet}$-$M^{\bullet}$, termination,

    v)   inclusion of the changes in the polymerization kinetic constants caused by increased viscosity, and finally

    vi)   inclusion of polymerization inhibiting effects.

The resulting Non-local Photo-polymerisation Driven Diffusion (NPDD) model was then experimentally verified by applying it to study (a) normalised transmission curves, and (b) growth curves of refractive index modulation for both short and continuous holographic exposures, in two significantly different free radical photopolymer materials [23,30-32]. The quality of the fits obtained to both photopolymer materials, indicated the versatility and applicability of the NPDD model.

In the past number of years, extensive work has been presented in the literature to describe the time varying absorption effects, which occur in photopolymer materials during exposure, [21,28,29]. In all cases the aim has been to improve the understanding of the photo-kinetics occurring in these materials, and critically to enable accurate predictions of the generation of primary radicals. A model of photosensitiser behaviour proposed by Carretero *et al.* [45], has recently been extended to account for: (i) photon absorption, (ii) the regeneration or recovery of absorptive photosensitiser, and (iii) photosensitiser bleaching, [46]. Using this model an expression for the time varying absorbed intensity, $I_a(t)$ (Einstein/cm^{3}s), was derived and the values of key material parameters were estimated using non-linear fits of the dye model to experimentally obtained transmission curves, [32]. The processes of primary radical generation were then described using the simple expression,
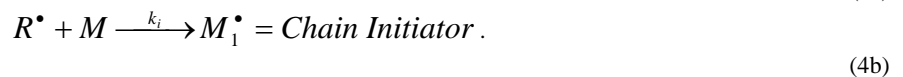
$$R_i = 2\Phi I_a(t),$$

(3)

where R_i is the rate of generation of primary radicals, Φ is the number of primary radicals initiated per photon absorbed. The factor of two indicates that radicals are created in pairs, [45-48].

We will now examine the methods used to extend the NPDD model in by more accurately representing the temporal and spatial variation of the photosensitiser concentration and the associated temporal and spatial generation and removal of primary radicals. As a result the number of approximations made in modelling the photo-initiation kinetics are significantly reduced. Thus a more physically accurate representation of the photo-polymerization kinetics is produced. Crucially, the increased physicality of the proposed model enables a more accurate analysis of the process of inhibition.
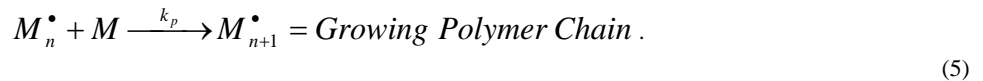
3.2 Reaction Mechanisms

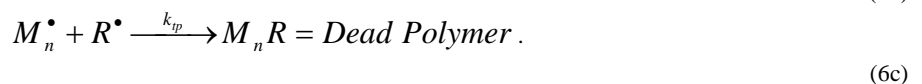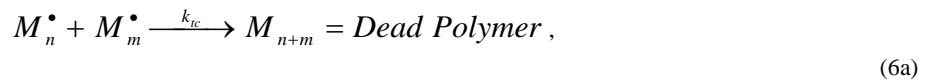The kinetic model presented in this analysis is based upon the following four reaction processes.
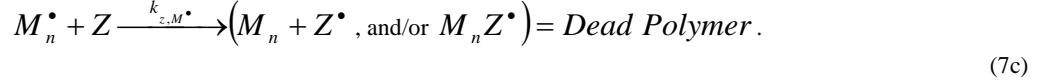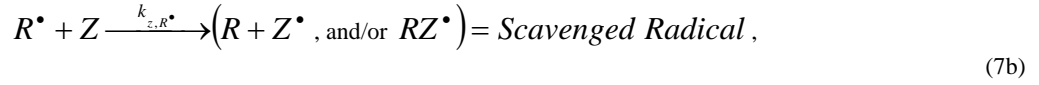
I.   **Initiation,**

$$I \xrightarrow{h\nu} R^{\bullet},$$

(4a)

$$R^{\bullet} + M \xrightarrow{k_i} M_1^{\bullet} = Chain\ Initiator.$$

(4b)

II.   **Propagation,**

$$M_n^{\bullet} + M \xrightarrow{k_p} M_{n+1}^{\bullet} = Growing\ Polymer\ Chain.$$

(5)

III.   **Termination,**

$$M_n^{\bullet} + M_m^{\bullet} \xrightarrow{k_{tc}} M_{n+m} = Dead\ Polymer,$$

(6a)

$$M_n^{\bullet} + M_m^{\bullet} \xrightarrow{k_{td}} M_n + M_m = Dead\ Polymer,$$

(6b)

$$M_n^{\bullet} + R^{\bullet} \xrightarrow{k_{tp}} M_n R = Dead\ Polymer.$$

(6c)

IV. **Inhibition**,

$$D^* + Z \xrightarrow{\ k_{z,Dye^*}\ } LeucoDye + Z^* ,$$

(7a)

$$R^\bullet + Z \xrightarrow{\ k_{z,R^\bullet}\ } \left(R + Z^\bullet \text{ , and/or } RZ^\bullet \right) = Scavenged\ Radical ,$$

(7b)

$$M_n^\bullet + Z \xrightarrow{\ k_{z,M^\bullet}\ } \left(M_n + Z^\bullet \text{ , and/or } M_n Z^\bullet \right) = Dead\ Polymer .$$
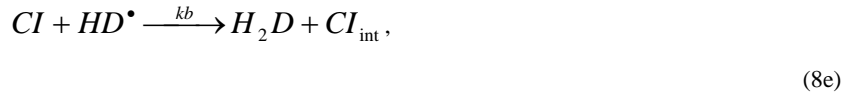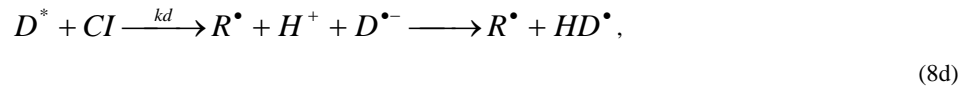
(7c)
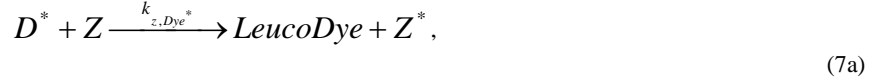
In the above set of chemical equations, I is the initiator concentration, $h\nu$ indicates the energy absorbed from a photon, M is the monomer concentration, Z is the inhibitor concentration, M_n, M_m, M_{n+m}, M_nR and $M_n Z^\bullet$ represent polymer species with no active propagating tip, i.e. *Dead Polymer*. D^* is the concentration of excited photosensitiser and Z^* is the concentration of singlet oxygen [38,40,48,49]. The term *Dead Polymer* signifies the cessation of the growth of a propagating macroradical of n monomer repeat units, [48], while the term *Scavenged Radical* signifies the removal of a primary radical, [38,48,49]. k_p, k_{tc}, k_{td}, $k_{z,M^\bullet}$, and

$k_{z,R^\bullet}$ (cm^{3}mol^{-1}s^{-1}) are the rate constants of propagation, termination by combination, termination by disproportionation, inhibition of macroradicals and inhibition of primary radicals respectively.

3.3 Primary Radical Production

As can be seen in Eq (4), the initiation process involves two steps: The ***first step*** is the production of free radicals by homolytic dissociation of the initiator to yield an initiator (primary) radical, $R^\bullet$, i.e., Eq (4a). The ***second step*** is chain initiation, i.e., Eq (4b), in which the primary radicals produced due to the absorption of photons react with the monomer to produce the chain initiating species

$M_1^\bullet$, [48]. The kinetic rate constant for this step is k_i (cm^{3}mol^{-1}s^{-1}), i.e. the chain initiation kinetic constant. As stated the main extensions to the previous model [30,31] involve improvements to the modelling of the temporal and spatial variations in primary radical production. Therefore, the main focus of this subsection will be the first step of the initiation mechanism, which is presented in Eq (4a).

In order to do this, we assume that the following photochemical reactions, take place upon illumination of a photopolymer layer sensitised with a xanthene or thiazine type photosensitiser [39], with an appropriate wavelength. These are as follows,

$$D + h\upsilon \xrightarrow{\ ka\ } D^* ,$$

(8a)

$$D^* + Z \xrightarrow{\ kz,D\ } Leuco\ Dye ,$$

(8b)

$$D^* \xrightarrow{\ kr\ } D ,$$

(8c)

$$D^* + CI \xrightarrow{\ kd\ } R^\bullet + H^+ + D^{\bullet -} \longrightarrow R^\bullet + HD^\bullet ,$$

(8d)

$$CI + HD^\bullet \xrightarrow{\ kb\ } H_2 D + CI_{int} ,$$

(8e)

In these equations D represents the concentration of photosensitiser (dye), $h\nu$ represents the photon energy incident on the material, D^* is the excited state of the dye, CI is the co-initiator, $R^\bullet$ represented the primary radical concentration, Z is the inhibitor, $HD^\bullet$ represents a radicalised dye, which has abstracted a hydrogen from the co-initiator, and H_2D is the di-hydro transparent form of the dye. CI_{int} is an intermediate form of the co-initiator, which is no longer available for reaction.

k_a (s^{-1}) is the rate of production of excited state photosensitiser, k_r (s^{-1}) is the rate of recovery or regeneration of photo-absorber, k_d (cm^{3}mol^{-1}s^{-1}) is the rate of dissociation of the initiator and $k_{z,D}$ (cm^{3}mol^{-1}s^{-1}) is the inhibition rate constant associated with the reaction with excited dye molecules. We note that previous models of the photo-initiation kinetics have not included all the reactions specified in Eq (8).

In order to use the proposed rate equations, it is first necessary to convert the exposure intensity I_0 (mW/cm^2) to the appropriate units (Einsteins/cm^{3}s). This can be done as follows, $I_0' = \dfrac{T_{sf} B I_0}{d}\left(\dfrac{\lambda}{N_a hc}\right)$, where λ (nm) is the wavelength of incident light, N_a (mol^{-1}) is Avogadro's constant, c (m/s) is the speed of light, and h (Js) is Plank's constant. $B = 1 - e^{-\varepsilon D_0 d}$, is the absorptive fraction which determines a material layer's initial absorptive capacity and is a function of the dye's initial concentration, T_{sf} is a fraction associated with the light lost by Fresnel and scattering losses, [29,32,45,46] D_0 (mol/cm^3), molar absorptivity, ε (cm^2/mol) and material layer thickness, d (cm).

The rate of production of the excited state photosensitiser, appearing in Eq (8a) can then be represented by $k_a = \phi \varepsilon d I_0'$ (s^{-1}), where ϕ (mol/Einstein) is the quantum efficiency of the reaction [48]. Therefore, if the photosensitiser's initial concentration, molar absorptivity, quantum efficiency, and layer thickness are known, the rate of generation of excited state photosensitiser, D^*, can be determined for a given exposure intensity.

3.4 Model Development

In the case of holographic illumination, i.e. to record a holographic grating, there is a spatial distribution of irradiance, which in our case is typically cosinusoidal. In this case the incident intensity is represented as $I(x,t) = I_0'[1 + V\cos(Kx)]$, where V is the fringe visibility and $K = 2\pi/\Lambda$, where Λ is the grating period. The mechanisms, which are presented in Eq (8), can then be represented by a set of coupled differential equations. The combination of these equations is equivalent to the previous representation of primary radical production in time and space, which is presented in Eq (3). Combining these coupled differential equations with those previously presented in Ref [30-32] for the mechanisms of initiation, propagation, termination and inhibition, yields the following set of first-order coupled differential equations governing the photosensitiser:

$$\frac{dD(x,t)}{dt} = -k_a D(x,t) + k_r D^*(x,t),$$

(9)

$$\frac{dD^*(x,t)}{dt} = k_a D(x,t) - k_r D^*(x,t) - k_d D^*(x,t) CI(x,t) - k_{z,D} D^*(x,t) Z(x,t),$$

(10)

$$\frac{dCI(x,t)}{dt} = -k_d D^*(x,t) CI(x,t) - k_b HD^\bullet(x,t) CI(x,t),$$

(11)

$$\frac{dHD^\bullet(x,t)}{dt} = k_d D^*(x,t) CI(x,t) - k_b HD^\bullet(x,t) CI(x,t),$$

(12)

As in the previous analysis, [30-32] it is assumed that the effect of inhibition during exposure is due solely to the initially dissolved oxygen present within the photopolymer layer. The non-uniform recording irradiance causes concentration gradients of oxygen as it is consumed in inhibitory reactions. This then results in the diffusion of oxygen from the dark non-illuminated regions to the bright illuminated regions. As oxygen molecules are small compared to the other material components which constitute the photopolymer layer, it can be assumed that the oxygen is relatively free to diffuse rapidly, resulting in a one-dimensional standard diffusion equation for the concentration of inhibitor,

$$\frac{dZ(x,t)}{dt} = \frac{d}{dx}\left[D_z \frac{dZ(x,t)}{dx}\right] - k_{z,D} D^*(x,t) Z(x,t)$$
$$- k_{z,R^\bullet} Z(x,t) R^\bullet(x,t) - k_{z,M^\bullet} Z(x,t) M^\bullet(x,t),$$

(13)

where Z is the instantaneous inhibiting oxygen concentration and D_z is the diffusion constant of oxygen in the dry material layer, which in this analysis will be assumed to be time and space independent. This assumption is reasonable, as this fast rate of diffusion of the small oxygen molecule will not be significantly affected by any small changes in material viscosity. The inhibition rate constants, $k_{z,R^\bullet}$ and $k_{z,M^\bullet}$, will in general have different values (of reactivity) due to the differences in the relative molecular size, [48]. However in this analysis, for the sake of simplicity we assume $k_z = k_{z,R^\bullet} = k_{z,M^\bullet}$. Furthermore it is expected that the reactivity of oxygen with the excited state form of the photosensitiser will be much lower, i.e. $k_{z,D} \ll k_z$ and therefore we assume it is negligible in this analysis. As before [30-32], it is assumed that the inhibition rate constant can be expressed as,

$$k_z = k_{z,0} \exp(-E_z/RT),$$

(14)

where in this equation $k_{z,0}$ (cm^{3}mol^{-1}s^{-1}) is the Arrhenius pre-exponential factor, $E_z = 18.23\times10^3$ (Jmol^{-1}) is the activation energy of oxygen, (i.e., the energy that must be overcome in order for oxygen to react with the given species), $R = 8.31$ (JK^{-1}mol^{-1}) is the universal gas constant, and T (K) is the local temperature [48].

The equation governing the concentration of primary radicals, including the new term for primary radical generation, is given by

$$\frac{dR^\bullet(x,t)}{dt} = k_d D^*(x,t)CI(x,t) - k_i R^\bullet(x,t)u(x,t) - k_{tp}R^\bullet(x,t)M^\bullet(x,t) - k_z R^\bullet(x,t)Z(x,t),$$

(15)

where $u(x, t)$ is the free-monomer concentration, (denoted earlier in the chemical reactions by M). This equation states that the rate of change of primary radical concentration is proportional to the concentration of primary radicals generated by photon absorption, minus the amounts removed by: (a) the initiation of macroradicals, (b) primary termination with growing polymer chains, and (c) inhibition by oxygen.

Including both types of termination mechanism (primary and bimolecular) and the effects of inhibition, the equation governing macroradical concentration is then

$$\frac{dM^\bullet(x,t)}{dt} = k_i R^\bullet(x,t)u(x,t) - 2k_t[M^\bullet(x,t)]^2 - k_{tp}R^\bullet(x,t)M^\bullet(x,t) - k_z Z(x,t)M^\bullet(x,t),$$

(16)

where the squared term represents the effects of bimolecular termination. The generation term in this equation previously appears as the removal term due to macroradical initiation in Eq (15).

The non-uniform irradiance creates monomer concentration gradients, and as a result monomer diffuses from the dark regions to the monomer depleted exposed regions. This results in a spatial polymer concentration distribution, which provides the modulation of refractive index in the material, i.e., the holographic grating. We represent the monomer concentration using the following 1D diffusion equation,

$$\frac{du(x,t)}{dt} = \frac{d}{dx}\left[D_m(x,t)\frac{du(x,t)}{dx}\right] - k_i R^\bullet(x,t)u(x,t) - \int_{-\infty}^{\infty} k_p M^\bullet(x',t)u(x',t)G(x,x')dx',$$

(17)

where $D_m(x, t)$ represents the monomer diffusion constant. $G(x,x')$ is the non-local material spatial response function given by [50]:

$$G(x, x') = \frac{1}{\sqrt{2\pi\sigma}} \exp\left[\frac{-(x-x')^2}{2\sigma}\right],$$

(18)

where σ is the constant non-local response parameter normalized with respect to the grating period, Λ. This non-local spatial response function represents the effect of initiation at location x' on the amount of monomer polymerized at location x.

The equation governing the polymer concentration is

$$\frac{dN(x,t)}{dt} = \int_{-\infty}^{\infty} k_p M^\bullet(x',t)u(x',t)G(x,x')dx' - \frac{d}{dx}\left[D_N(x,t)\frac{dN(x,t)}{dx}\right],$$

(19)

where $D_N(x, t)$ represents the polymer diffusion constant. As with the monomer above in Eq (17), the non-uniform irradiance creates a polymer concentration distribution. If the polymer chains are not cross-linked sufficiently, they will tend to diffuse out of the exposed regions in order to reduce the polymer gradient, [29]. If this takes place it will result in a decay of the grating strength with time. However here we assume there is sufficient cross-linking and that $D_N(x,t) = 0$, i.e., we record very stable gratings, as seen in the analysis presented in Ref [29], which uses the same material composition.

Since all the above equations presented in Eqs (9–13), (15-17) and (19), depend upon the spatial distribution of the exposing intensity, they will all be periodic even functions of x and can therefore be written as Fourier series, i.e.,

$$X(x,t) = \sum_{j=0}^{\infty} X_j(t)\cos(jKx),$$ where X represents the species concentrations, D, D^*, CI, $HD^\bullet$, $R^\bullet$, $M^\bullet$, u, N and Z. A set of

first-order coupled differential equations can then be obtained in the same manner presented in Refs [30-32], by gathering the coefficients of the various co-sinusoidal spatial contributions and writing the equations in terms of these time varying spatial harmonic amplitudes. These coupled equations can then be solved using the following initial conditions,

$$Z_0(t=0) = Z_0, \ D_0(t=0) = D_0, \ CI_0(t=0) = CI_0, \ u_0(t=0) = U_0,$$
$$D_{n>0}(t=0) = D^*_{n\geq0}(t=0) = HD^\bullet_{n\geq0}(t=0) = CI_{n>0}(t=0) = 0, \text{ and}$$
$$Z_{n>0}(t=0) = R^\bullet_{n\geq0}(t=0) = M^\bullet_{n\geq0}(t=0) = N_{n\geq0}(t=0) = 0.$$

(20)

As in previous analysis the Fourier series expansion of the monomer and polymer harmonics involves use of the non-local response parameter $G(x,x')$ which is represented in the coupled differential equations by $S_i = \exp(-i^2 K^2 \sigma / 2)$.

3.5 Model Simulations

In order to examine the general behaviour of this model, we now generate a number of theoretical simulations and analyse their predictions. In all theoretical simulations presented here, it is assumed that time varying viscosity effects are negligible and therefore, $D_m(x,t) = D_{m0} = 8.0 \times 10^{-11}$ cm^2/s. All kinetic parameter values are assigned appropriate values, which are typical for the AA/PVA photopolymer material examined here, [30-32].

12 spatial concentration harmonics are retained in the simulations, solved using the initial conditions presented in Eq (20) with $U_0 = 2.83 \times 10^{-3}$ mol/cm^3, $D_0 = 1.22 \times 10^{-6}$ mol/cm^3, $CI_0 = 3.18 \times 10^{-3}$ mol/cm^3 and $Z_0 = 1 \times 10^{-8}$ mol/cm^3. Assuming typical recording conditions for an unslanted transmission type volume holographic grating, for $\Lambda = 700$ nm and fringe visibility $V = 1$, simulations of the temporal and spatial variation in the photosensitiser concentration, $D(x,t)$, are generated and presented in Figure 2a. The typical rate constants used were $k_p = k_i = 2.65 \times 10^7$ cm^3/mol s, $k_t = 6 \times 10^9$ cm^3/mol s, $k_{tp} = k_t \times 10$, $k_d = k_b = 1.6 \times 10^3$ cm^3/mol s, $k_z = 3 \times 10^{12}$ cm^3/mol s and $k_r = 1.22 \times 10^{-3}$ s^{-1}, [30-32]. For an exposure intensity of $I_0 = 1$ mW/cm^2 and $\lambda = 532$ nm, the absorption parameters estimated from fits to normalised transmission curves for a material layer of thickness $d = 100$ μm were, $\varepsilon = 1.4 \times 10^8$ cm^2/mol, $\phi = 0.066$ mol/Einstein and $T_{sf} = 0.76$, with $N_a = 6.02 \times 10^{23}$ mol^{-1}, $c = 3 \times 10^8$ ms^{-1} and $h = 6.62 \times 10^{-34}$ Js, [32]. The oxygen diffusion coefficient was assumed to be $D_z = 1.0 \times 10^{-8}$ cm^2/s, [51]. The parameter S_1, which quantifies the extent of the non-locality in the first harmonic coupled differential equation, was chosen to have a value of $S_1 = 0.94$, [29,50]. This corresponds to a non-local response length of $\sqrt{\sigma'} = 54$ nm, [29].

As can be observed from Figure 2, the spatial sinusoidal variation in the exposing interference pattern causes a rapid consumption of the ground state dye in the bright illuminated regions. As the exposure time increases the sinusoidal variation of the dye concentration is distorted and the width of the non-illuminated dark bands narrows. This loss in sinusoidal fidelity results in a spatial production of primary radicals, as shown in Figure 3, which deviates significantly from the sinusoidal primary radical generation which would be generated using the term presented in Eq (3). Subsequently, this yields a non-linear material response, as the number of polymer chains initiated are not simply generated in direct proportion to the exposing interference pattern. This is an important prediction of the model, which agrees well with experimental observation.
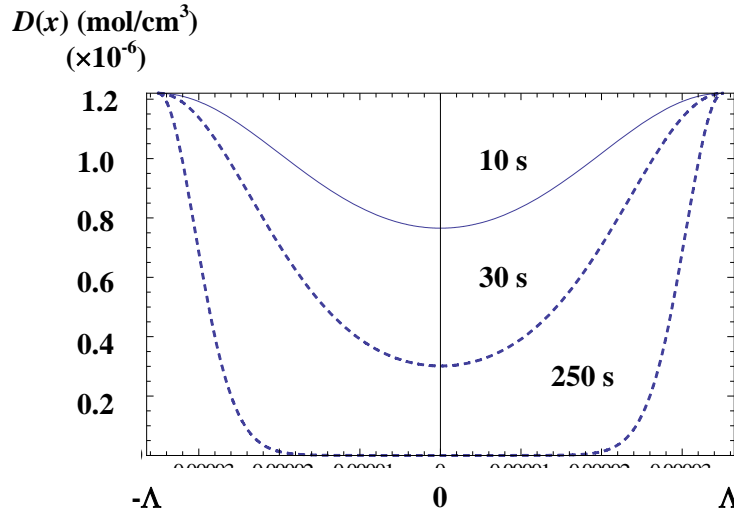

Figure 2. Simulation of the spatial variation of the ground state photosensitiser concentration for an exposure intensity $I_0 = 1$mW/cm^2, at $\Lambda = 700$ nm, for various exposure times, $t_{exp} = 10$s (joined line), $t_{exp} = 30$s (small dashed line), $t_{exp} = 250$s (dashed line).

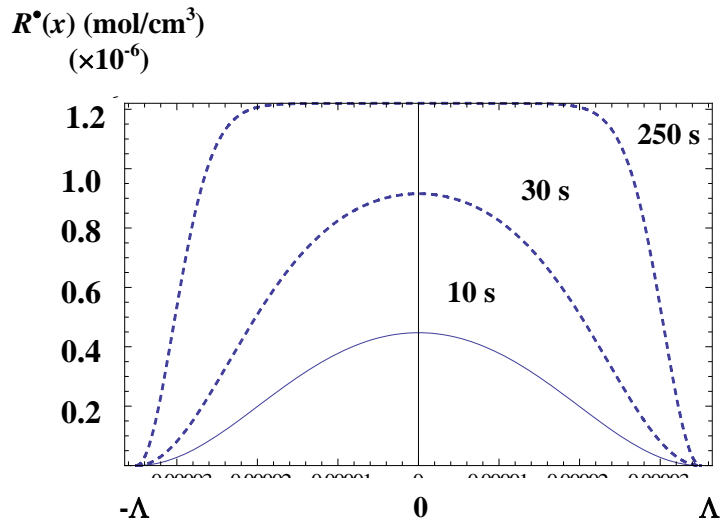Figure 3. Simulation of the spatial variation of the generation of primary radicals for an exposure intensity $I_0 = 1\text{mW/cm}^2$, at $\Lambda = 700$ nm, for various exposure times, $t_{\text{exp}} = 10\text{s}$ (joined line), $t_{\text{exp}} = 30\text{s}$ (small dashed line), $t_{\text{exp}} = 250\text{s}$ (dashed line).

Using the same parameter values used to generate Figures 2 and 3, Figure 4 shows a simulation of the amplitudes of the first two concentration harmonics of the monomer, u_0 and u_1, and the corresponding polymer variations, N_0 and N_1. The presence of a 'deadband' or inhibition period, t_i, can be observed at the early stages of exposure as a result of the inhibitory reactions. This behaviour is consistent with the reaction mechanisms discussed in earlier, where the primary- and macro-radicals are scavenged by oxygen, which is initially dissolved in the photopolymer layer.
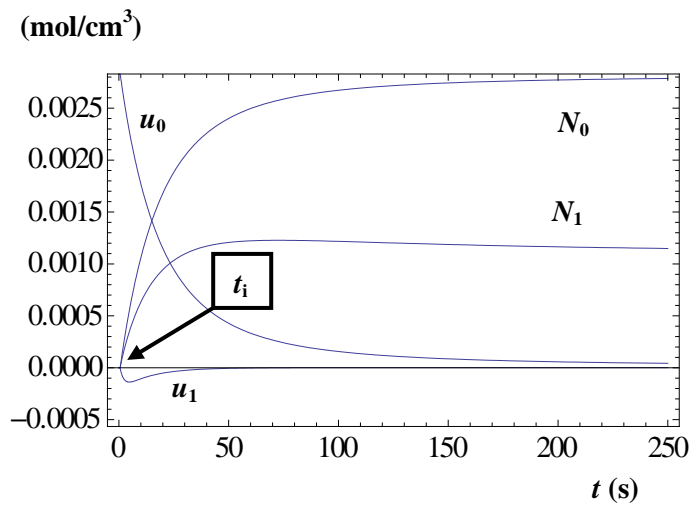

Figure 4. Simulations of the variation of the first two concentration harmonics of monomer and polymer using the theoretical model.

Figure 5, shows a simulation of growth curves of refractive index modulation with varying values of the concentration of initially dissolved oxygen, Z_0 (mol/cm^3), under the same conditions as the previous figures but with $Z_0 = 1 \times 10^{-8}$ mol/cm^3 (joined line), $Z_0 = 5 \times 10^{-8}$ mol/cm^3 (short dashed line), and $Z_0 = 1 \times 10^{-7}$ mol/cm^3 (long dashed line). As the concentration of inhibitor is increased, the inhibition time, t_i increases as expected, i.e., more inhibitor causes a greater scavenging of the primary- and macro-radicals.
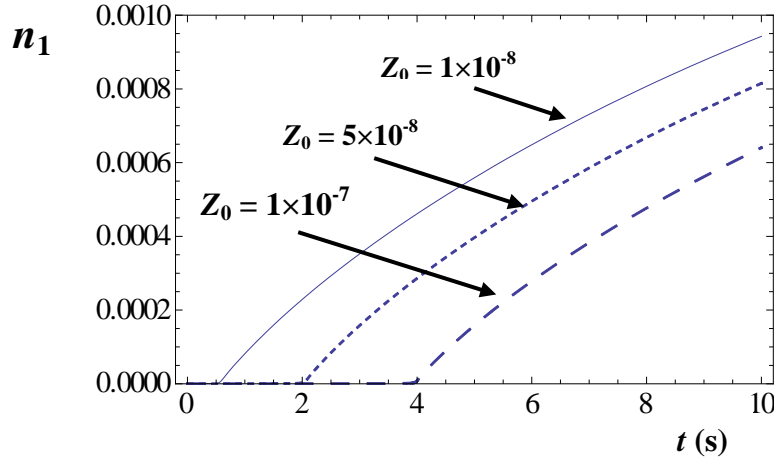
Figure 5. Simulations of the refractive index modulation with time, for various values of dissolved oxygen concentration. $Z_0 = 1 \times 10^{-7}$ mol/cm^3 (long dashed line), $Z_0 = 5 \times 10^{-8}$ mol/cm^3 (short dashed line) and $Z_0 = 1 \times 10^{-8}$ mol/cm^3 (joined line).

When comparing the experimental results obtained using the optical setup described above with the theoretical predictions generated by the extended model, it became clear that when using the model as presented, the trend of increased inhibition times, t_i, for reduced exposure intensities, did not satisfactorily replicate the experimental behavior observed. In order to achieve good fits to the experimental data, it was found necessary to increase the initial concentration of dissolved oxygen available in the photopolymer layer, Z_0, as the recording intensities were reduced. The variation between the experimental observation and theoretical prediction was as much as 8 s for the lowest recording intensity examined for unsealed photopolymer layers (not sealed from the environment). This divergence between experiment and prediction suggested that the model was incomplete and, that in order to mimic this physically observed behavior, amendments to the model were necessary.

In a previous paper published by the authors [49], it was found that by cover-plating or sealing the photopolymer layer with glass slides, the inhibition times observed during exposure compared with the uncoverplated or unsealed layers, were significantly reduced. These effects were attributed to the removal or reduction of oxygen diffusing in from the surrounding environment, which was replacing or replenishing the oxygen consumed during exposure. It must be noted at this point, that the experimental data examined here were uncoverplated photopolymer layers, which were subject to this potential external oxygen diffusion.

In order to represent this process in the model, an additive term representing the replenishing of inhibiting oxygen from the outside surrounding air, into the material layer, was included. Therefore, Eq (13) was revised and became,

$$\frac{dZ(x,t)}{dt} = \frac{d}{dx}\left[D_z \frac{dZ(x,t)}{dx} \right] - k_{z,D} D^*(x,t)Z(x,t) - k_{z,R} \cdot Z(x,t)R^\bullet(x,t)$$

$$- k_{z,M} \cdot Z(x,t)M^\bullet(x,t) + \tau_z\left[Z_0 - Z(x,t) \right],$$

(21)

where τ_z represents the rate of replenishing of oxygen into the material layer. We note that it is assumed that the oxygen concentration can never be larger than the original dissolved oxygen concentration, Z_0 (mol/cm^3) and that this additive term is assumed to be constant in space.

In order to illustrate these effects Figure 6 shows a simulation of the behavior of the oxygen concentration with varying values of the replenishing constant, τ_z, for an exposure intensity, $I_0 = 0.04$ mW/cm^2 and exposure time, $t_{exp} = 30$ s. As can be observed, an increase in τ_z results in: (i) an increase of the inhibition period, and (ii) an increase in the rate at which oxygen returns to its original dissolved oxygen concentration, post-exposure.
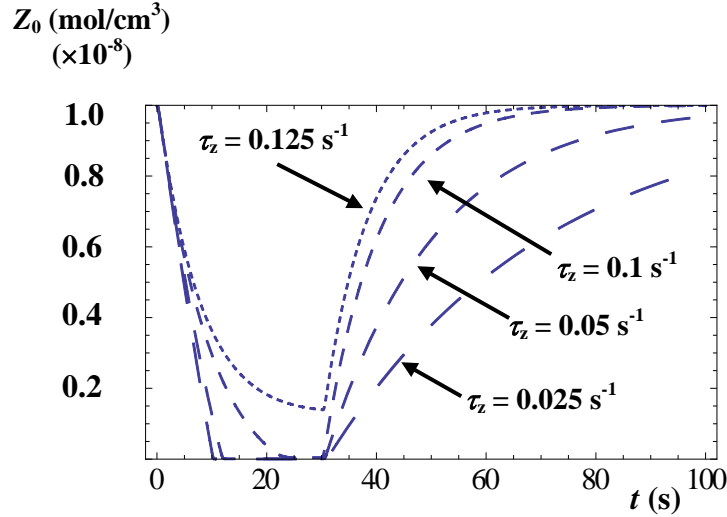
Figure 6. Simulation of the behaviour of the oxygen concentration with varying values of τ_z, for an exposure time, $t_{exp} = 30$ s and exposure intensity, $I_0 = 0.04$ mW/cm^2. $\tau_z = 0.125$ s^{-1} (shortest dash), $\tau_z = 0.1$ s^{-1} (short dash), $\tau_z = 0.05$ s^{-1} (long dash), $\tau_z = 0.025$ s^{-1} (longest dash).

Implementing the appropriate Fourier series expansion to Eq (21) under the same initial conditions, the model is then applied to the experimental growth curves recorded in uncoverplated layers, yielding much more accurate fits to the data. Figure 7 shows a subset of this data with the corresponding fits obtained using the model. Some of the parameter values which were obtained from the fits to various intensities are, $k_d = 1.6 \times 10^3$ cm^3/mol s, $k_r = 1.2 \times 10^{-3}$ s^{-1}, $k_z = 3.0 \times 10^{12}$ cm^3/mol s, $D_z = 1 \times 10^{-8}$ cm^2/s, and it was assumed in all fits that $k_{tp} = 10 \times k_t$ cm^3/mol s, and $k_i = k_p$ cm^3/mol s.
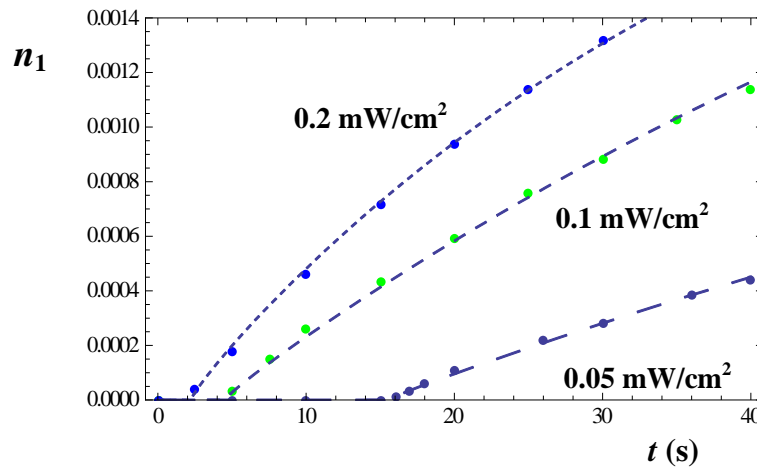

Figure 7. Experimentally obtained growth curves of refractive index modulation recorded in uncoverplated AA/PVA photopolymer material layers at a spatial frequency of 1428 lines/mm for 3 different exposing intensities, $I_{01} = 0.2$ mW/cm^2 (short dash), $I_{02} = 0.1$ mW/cm^2 (dashed) and $I_{03} = 0.05$ mW/cm^2 (long dash) with corresponding fits achieved with the theoretical model.

The most significant values extracted from the fits are presented in Table 1 along with the parameter search ranges, which were used to obtain a best fit between experimental and theoretical prediction. These search ranges are typical of the valued presented in the literature for similar photopolymer materials, [42,48,51]. The Mean Squared Error (MSE) between the fit and the data are also included to indicate the quality of the fits.

I_0 (mW/cm^2)	t_i (s)	k_p (cm^3/mols) ($\times 10^7$)	k_t (cm^3/mols) ($\times 10^9$)	D_{m0} (cm^2/s) ($\times 10^{-11}$)	τ_z (s^{-1})	MSE ($\times 10^{-11}$)
0.20	2.50	2.42	5.0	8.0	0.075	1.05
0.10	4.50	2.52	7.0	9.0	0.080	2.86
0.05	16.00	3.00	7.0	10.0	0.115	1.88
Search Range	-	0.1 - 5.0	0.1 - 9.0	1.0 – 12.0	-	-

Table 1. Parameters extracted from fits to experimentally obtained growth curves of refractive index modulation in uncoverplated photopolymer layers.

As can be observed from Figure 7, the fit quality is very good and the model predicts the observed trend, that a reduction in the exposure intensity causes an increase in the inhibition period due to (i) initially dissolved oxygen and (ii) oxygen diffusion into the material from the surrounding air. It can also be seen that there is a reduction in the propagation and termination rates with increasing exposure intensities. This is most likely due to the increased viscosity effects, which occur due to increased conversion of monomer to polymer [48]. This is consistent with the results obtained from the previous model, [30-32]. It must also be noted at this point that the estimates obtained for the rates of propagation and termination are slightly higher than those reported in the previous published work by the authors, [30-32]. This is as a result of a more physically accurate description of the primary radical generation introduced by the model development. However, the estimated values extracted from the fits still remain well within the accepted ranges presented in the literature for similar photopolymer materials.

In order to verify the necessity for the inclusion of the additive oxygen replenishing term in Eq (21), several growth curves of refractive index modulation were recorded in coverplated layers. These growth curves were recorded under the same conditions as the uncoverplated layers presented in Figure 7. Figure 8 shows experimental growth curves recorded at an exposure intensity of $I_0 = 0.05$ mW/cm^2, in both coverplated and uncoverplated layers. The subsequent fits to the experimental data, which were achieved using the revised model are represented as short dash line (coverplated) and long dash line (uncoverplated).
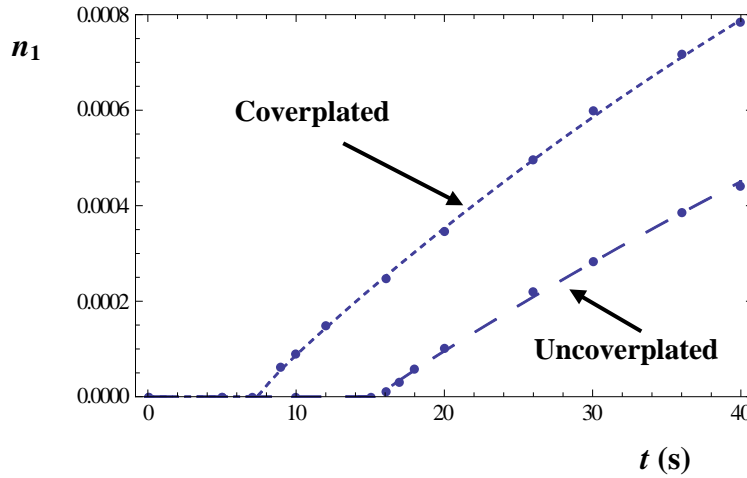

Figure 8. Experimentally obtained growth curves of refractive index modulation recorded in both coverplated (short dash) and uncoverplated (long dash) AA/PVA photopolymer material layers at a spatial frequency of 1428 lines/mm for a recording intensity $I_0 = 0.05$ mW/cm^2 with corresponding fits achieved with the model.

As can be observed from the figure there is a significant reduction in the inhibition period, from $t_i = 16$ s (uncoverplated) to $t_i = 9$s (coverplated). As stated above, this is attributed to a reduction in the amount of oxygen available to diffuse into the layer from the surrounding air. The estimated parameters extracted from these fits are presented in Table 2. The values determined for the replenishing rate τ_z, are consistent with what is experimental observed. In the case of the coverplated material layer, it is assumed that no oxygen can diffuse into the layer, i.e. $\tau_z = 0$.

	t_i (s)	k_p (cm³/mols) (×10⁷)	k_t (cm³/mols) (×10⁹)	D_{m0} (cm²/s) (×10⁻¹¹)	τ_z (s⁻¹)	MSE (×10⁻¹¹)
Coverplated	9.0	2.9	7.0	10.0	0.000	2.26
Uncoverplated	16.0	3.0	7.0	10.0	0.115	1.88
Search Range	-	0.1 - 5.0	0.1 - 9.0	1.0 - 12.0	-	-

Table 2. Parameters extracted from fits to experimentally obtained growth curves recorded at $I_0 = 0.05$mW/cm² for a coverplated and uncoverplated polymer layer.

In this section, further developments of the Non-local Photo-polymerization Driven Diffusion (NPDD) model, were presented. For the first time, the spatial and temporal variations in primary radical generation were included. These extensions provided a more physically comprehensive theoretical representation of the processes, which occur during free radical photo-polymerization. A clearer more physical representation of the reactions, which take place during the photo-initiation stages, was also provided, including the spatial and temporal consumption and regeneration of the photosensitiser and the reactions between the excited dye molecules and the co-initiator. Simulations were presented, which highlight the loss of sinusoidal fidelity of the primary radical generation. This behaviour deviates from that which was previously predicted in the literature. Subsequently, this change in the spatial generation of primary radicals has a substantial effect on the distribution of the polymer chains formed and hence, on the resulting refractive index modulation recorded.

The model was then further extended to incorporate the effect of oxygen diffusion from outside the material layer by including a rate of oxygen replenishing. This allowed accurate modelling of the inhibition effects, which dominate the start of grating growth. The results obtained were consistent with previous studies where cover-plating techniques were used.

In the following section, we will examine the effects of adding chain transfer agents to an AA/PVA photopolymer material in order to reduce the average polymer chain length grown during grating fabrication. This will then cause a reduction in the extent of the non-local chain growth of these polymer chains and thus reduce the fall off in refractive index modulation at higher spatial frequencies.
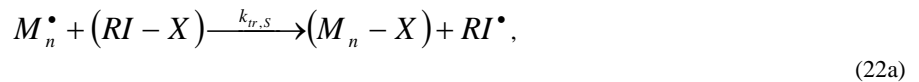
4.   IMPROVING THE SPATIAL FREQUENCY RESPONSE OF PHOTOPOLYMERS

The non-local spatial response function presented in Eq (18) (in Section 3.4) represents the effect of a chain initiation at location x' on the amount of monomer polymerized at location x, [50], where σ is the constant non-local response parameter which is normalized with respect to the period of the grating being recorded, Λ This is an important parameter when considering the data storage capacity or high density resolution of a photopolymer. The Non-local Photo-Polymerization Driven Diffusion (NPDD) model predicts that a reduction in this non-local response parameter within a photopolymer material will improve its high spatial frequency response. A point to note is that the non-local response of a given photopolymer is produced by a combination of several physical effects, which result in the smearing of the grating being recorded in the photopolymer. One such smearing effect is this growth of polymer chains away from the point of their initiation, into the dark less exposed regions of the material layer. This propagation out of the bright regions causes an increase in the average refractive index of the dark region and as a result, reduces the overall refractive index modulation achievable. This has been illustrated in discussed in detail in previous publications [29-31,50], and is more significant when recording high spatial frequency.

The introduction of a chain transfer agent acts to reduce the average molecular weight of polymer chains grown during free radical polymerization. Therefore a chain transfer agent (CTA) can provide a practical method to reduce the non-local response length. In this section an extended NPDD model is presented, which includes the chain transfer reactions and all major photochemical processes.

4.1 Chain Transfer Mechanism
In many polymerization systems, the average polymer weight is observed to be lower than predicted by the chain transfer reaction [29,52-55]. Generally, the chain transfer process causes the premature termination of a growing macro-radical chain and arises because of the presence of CTA [48]. Due to this reaction, a new radical is produced which is referred to in this work as a re-initiator. This re-initiator reacts with a monomer molecule to initiate a new growing macro-radical chain. Therefore we can write the chain transfer reactions as,

$$M_n^\bullet + \left(RI - X\right) \xrightarrow{\ k_{tr,S}\ } \left(M_n - X\right) + RI^\bullet,$$

(22a)

$$RI^\bullet + M \xrightarrow{\ k_{ri}\ } \left(RI - M^\bullet\right),$$

(22b)

where RI-X is the chain transfer agent, $-X$ is the atom or species transferred and $RI^\bullet$ is the re-initiator which has a radical tip. $k_{tr,S}$ and k_{ri} are the transfer rate constant to chain-transfer agent and the re-initiation rate constant respectively. Due to the premature termination reaction with the chain transfer agent, RI-X, the propagating polymer chains will stop growing earlier than they would

have if the CTA was not present. We assume that the free radical $RI\text{-}M^\bullet$ produced can be treated as acting chemically identical to a chain initiator $M^\bullet$. Therefore the re-initiator, $RI^\bullet$, simply initiates a new growing chain with a radical tip, $M^\bullet$. Thus, while the polymer chains are shortened, the amount of monomer polymerized and the rate of polymerization can remain high.

In the radical chain polymerization system [29,48], the polymerization rate can be expressed as:

$$R_P = k_p M^\bullet(x,t) u(x,t).$$

(23)

The polymerization rate, R_p, is also related to the number-average degree of polymerization, DP_n. DP_n is defined as the average number of structural units per polymer chain. It indicates the average length of polymer chain grown and therefore their molecular weight. According to the *Mayo Equation* [48,52],

$$\frac{1}{DP_n} = \frac{k_t R_p}{k_p^2 [u]^2} + C_u + C_{CTA} \frac{[CTA]}{[u]} + C_I \frac{[I]}{[u]}.$$

(24)

This quantifies the effect of the various chain transfer reactions on the number-average degree of polymerization. $[u]$, $[CTA]$, $[I]$, represent the concentrations of monomer, chain transfer agent and initiator, respectively. The chain-transfer constants, C_u, C_{CTA} and C_I, for each particular substance are defined as the ratios of the rate constants for chain transfer of a propagating radical with that substance to the propagation rate constant, k_p. They can be expressed as:

$$C_u = \frac{k_{tr,u}}{k_p}, \ \ C_{CTA} = \frac{k_{tr,CTA}}{k_p}, \text{ and } C_I = \frac{k_{tr,I}}{k_p},$$

(25)

where $k_{tr,u}$, $k_{tr,CTA}$, $k_{tr,I}$ represent rate constants for chain transfer to monomer, to chain transfer agent and to initiator respectively. For the case examined here the chain transfer constants to monomer and initiator, can be omitted as they are typically very low for acrylamide [56,57], and therefore Eq. (24) can be simplified to:

$$\frac{1}{DP_n} = \frac{k_t R_p}{k_p^2 [u]^2} + C_{CTA} \frac{[CTA]}{[u]},$$

(26)

which will be discussed in detail in next section.

4.2   Model Development

In order to begin to examine the effects of the presence of CTA on the material non-local response length, $\sqrt{\sigma}$, (the actual physical length of the nonlocal response parameter, units of nanometres) we introduce a rate equation governing the CTA concentration:

$$\frac{d[CTA(x,t)]}{dt} = \frac{d}{dx}\left\{ D_{CTA}(x,t) \frac{d[CTA(x,t)]}{dx} \right\} - k_{tr,S}[CTA(x,t)]\,[M^\bullet(x,t)].$$

(27)

It should be noted that, in the following analysis, we only consider chain transfer to chain-transfer agent, i.e., the chain transfer constants for monomer and initiator are assumed negligible. To further simplify the analysis in this work, we assume that $k_{tr} = k_{tr,CTA}$ and that the CTA diffusion rate, D_{CTA}, is similar to the diffusion rate of monomer, D_m, as their molecular weights are similar in the cases examined, i.e., $D_{CTA} \approx D_m$.

The equation governing the re-initiator concentration can be given by,

$$\frac{d[RI^\bullet(x,t)]}{dt} = k_{tr}[CTA(x,t)]\,[M^\bullet(x,t)] - k_{ri}[RI^\bullet(x,t)]\,[u(x,t)],$$

(28)

where $RI^\bullet$ denotes the re-initiator concentration. Since it is assumed that the initiator radical, $R^\bullet$, dominates the primary termination and inhibition processes, we only consider how the re-initiator, $RI^\bullet$, reacts with the monomer.

Furthermore the chain transfer and re-initiation reactions effect the variation of macro-radical, $[M^\bullet]$, and monomer, $[u]$, concentrations. Therefore we must change the coupled differential equations for monomer and macroradicals presented earlier in Section 3, giving,

$$\frac{d[M^\bullet(x,t)]}{dt} = k_i[R^\bullet(x,t)]\,[u(x,t)] + k_{ri}[RI^\bullet(x,t)]\,[u(x,t)] - 2k_t[M^\bullet(x,t)]^2$$
$$- k_{tp}[R^\bullet(x,t)]\,[M^\bullet(x,t)] - k_z[Z(x,t)]\,[M^\bullet(x,t)] - k_{tr}[CTA(x,t)]\,[M^\bullet(x,t)],$$

(29)

and,

$$\frac{d[u(x,t)]}{dt} = \frac{d}{dx}\left\{D_m(x,t)\frac{d[u(x,t)]}{dx}\right\} - k_i\left[R^\bullet(x,t)\right][u(x,t)]$$
$$- \int_{-\infty}^{\infty} k_p\left[M^\bullet(x',t)\right][u(x',t)]G(x,x')dx' - k_{ri}\left[RI^\bullet(x,t)\right][u(x,t)].$$

(30)

As before the concentrations of the components of the photopolymer and the amended equations appearing here in Eqs (27–30) will be periodic even functions of x and can therefore be written as Fourier series, i.e., $[X(x,t)] = \sum_{j=0}^{\infty} X_j(t)\cos(jKx)$, where X represents the particular species, i.e., CTA, $RI^\bullet$, $M^\bullet$, and u. A set of first-order coupled differential equations can then be obtained by gathering the coefficients of the various co-sinusoidal spatial components and writing the equations in terms of these time varying spatial harmonic amplitudes, $X_j(t)$.

For brevity we will assume here that harmonics of order greater than $j = 3$, are negligible and for illustration purposes we now present the first two harmonics of $[CTA]$, $[RI^\bullet]$, $[M^\bullet]$, and $[u]$, all of which are directly involved in reactions with the transfer agent.

Chain Transfer Agent Concentration: Retaining the first four concentration harmonic amplitudes in the analysis, the following first-order coupled differential equations govern the chain transfer agent concentration amplitudes, CTA_j:

$$\frac{dCTA_0(t)}{dt} = -k_{tr}CTA_0(t)M_0^\bullet(t) - \frac{1}{2}k_{tr}CTA_1(t)M_1^\bullet(t) - \frac{1}{2}k_{tr}CTA_2(t)M_2^\bullet(t)$$
$$- \frac{1}{2}k_{tr}CTA_3(t)M_3^\bullet(t),$$

(31a)

$$\frac{dCTA_1(t)}{dt} = -D_{CTA}K^2CTA_1(t) - k_{tr}CTA_1(t)M_0^\bullet(t) - k_{tr}CTA_0(t)M_1^\bullet(t)$$
$$- \frac{1}{2}k_{tr}CTA_2(t)M_1^\bullet(t) - \frac{1}{2}k_{tr}CTA_1(t)M_2^\bullet(t)$$
$$- \frac{1}{2}k_{tr}CTA_3(t)M_2^\bullet(t) - \frac{1}{2}k_{tr}CTA_2(t)M_3^\bullet(t),$$

(31b)

Re-initiator Concentration: The equations governing the re-initiator concentration amplitudes, $RI_j^\bullet$, are:

$$\frac{dRI_0^\bullet(t)}{dt} = k_{tr}CTA_0(t)M_0^\bullet(t) + \frac{1}{2}k_{tr}CTA_1(t)M_1^\bullet(t) + \frac{1}{2}k_{tr}CTA_2(t)M_2^\bullet(t)$$
$$+ \frac{1}{2}k_{tr}CTA_3(t)M_3^\bullet(t) - k_{ri}RI_0^\bullet(t)u_0(t) - \frac{1}{2}k_{ri}RI_1^\bullet(t)u_1(t)$$
$$- \frac{1}{2}k_{ri}RI_2^\bullet(t)u_2(t) - \frac{1}{2}k_{ri}RI_3^\bullet(t)u_3(t),$$

(32a)

$$\frac{dRI_1^\bullet(t)}{dt} = k_{tr}CTA_1(t)M_0^\bullet(t) + k_{tr}CTA_0(t)M_1^\bullet(t) + \frac{1}{2}k_{tr}CTA_2(t)M_1^\bullet(t)$$
$$+ \frac{1}{2}k_{tr}CTA_1(t)M_2^\bullet(t) + \frac{1}{2}k_{tr}CTA_3(t)M_2^\bullet(t) + \frac{1}{2}k_{tr}CTA_2(t)M_3^\bullet(t)$$
$$- k_{ri}RI_1^\bullet(t)u_0(t) - k_{ri}RI_0^\bullet(t)u_1(t) - \frac{1}{2}k_{ri}RI_2^\bullet(t)u_1(t)$$
$$- \frac{1}{2}k_{ri}RI_1^\bullet(t)u_2(t) - \frac{1}{2}k_{ri}RI_3^\bullet(t)u_2(t) - \frac{1}{2}k_{ri}RI_2^\bullet(t)u_3(t),$$

(32b)

Macro-radical Concentration: From Eq. (29), equations governing the $M_j^\bullet$, are:

$$\frac{dM_0^\bullet(t)}{dt} = -\frac{k_{tr}}{2}\left[2CTA_0(t)M_0^\bullet(t) + CTA_1(t)M_1^\bullet(t) + CTA_2(t)M_2^\bullet(t)\right.$$

$$\left. + CTA_3(t)M_3^\bullet(t)\right] - \frac{k_t}{2}\left[2M_0^\bullet(t)^2 + M_1^\bullet(t)^2 + M_2^\bullet(t)^2 + M_3^\bullet(t)^2\right]$$

$$-\frac{k_{tp}}{2}\left[2M_0^\bullet(t)R_0^\bullet(t) + M_1^\bullet(t)R_1^\bullet(t) + M_2^\bullet(t)R_2^\bullet(t) + M_3^\bullet(t)R_3^\bullet(t)\right]$$

$$-\frac{k_z}{2}\left[2M_0^\bullet(t)Z_0(t) + M_1^\bullet(t)Z_1(t) + M_2^\bullet(t)Z_2(t) + M_3^\bullet(t)Z_3(t)\right]$$

$$+\frac{k_i}{2}\left[2R_0^\bullet(t)u_0(t) + R_1^\bullet(t)u_1(t) + R_2^\bullet(t)u_2(t) + R_3^\bullet(t)u_3(t)\right]$$

$$+\frac{k_{ri}}{2}\left[2RI_0^\bullet(t)u_0(t) + RI_1^\bullet(t)u_1(t) + RI_2^\bullet(t)u_2(t) + RI_3^\bullet(t)u_3(t)\right],$$

$$(33a)$$

$$\frac{dM_1^\bullet(t)}{dt} = -\frac{k_{tr}}{2}\left[2CTA_1(t)M_0^\bullet(t) + 2CTA_0(t)M_1^\bullet(t) + CTA_2(t)M_1^\bullet(t)\right.$$

$$\left. + CTA_1(t)M_2^\bullet(t) + CTA_3(t)M_2^\bullet(t) + CTA_2(t)M_3^\bullet(t)\right]$$

$$- k_t\left[2M_0^\bullet(t)M_1^\bullet(t) + M_1^\bullet(t)M_2^\bullet(t) + M_2^\bullet(t)M_3^\bullet(t)\right]$$

$$-\frac{k_{tp}}{2}\left[2M_1^\bullet(t)R_0^\bullet(t) + 2M_0^\bullet(t)R_1^\bullet(t) + M_2^\bullet(t)R_1^\bullet(t) + M_1^\bullet(t)R_2^\bullet(t)\right.$$

$$\left. + M_3^\bullet(t)R_2^\bullet(t) + M_2^\bullet(t)R_3^\bullet(t)\right]$$

$$-\frac{k_z}{2}\left[2M_1^\bullet(t)Z_0(t) + 2M_0^\bullet(t)Z_1(t) + M_2^\bullet(t)Z_1(t) + M_1^\bullet(t)Z_2(t)\right.$$

$$\left. + M_3^\bullet(t)Z_2(t) + M_2^\bullet(t)Z_3(t)\right]$$

$$+\frac{k_i}{2}\left[2R_1^\bullet(t)u_0(t) + 2R_1^\bullet(t)u_0(t) + R_2^\bullet(t)u_1(t) + R_1^\bullet(t)u_2(t)\right.$$

$$\left. + R_3^\bullet(t)u_2(t) + R_2^\bullet(t)u_3(t)\right]$$

$$+\frac{k_{ri}}{2}\left[2RI_1^\bullet(t)u_0(t) + 2RI_1^\bullet(t)u_0(t) + RI_2^\bullet(t)u_1(t) + RI_1^\bullet(t)u_2(t)\right.$$

$$\left. + RI_3^\bullet(t)u_2(t) + RI_2^\bullet(t)u_3(t)\right],$$

$$(33b)$$

Monomer Concentration: The coupled equations for the monomer concentration harmonics, u_j, are:

$$\frac{du_0(t)}{dt} = -\frac{k_p}{2}\left[2M_0^\bullet(t)u_0(t) + M_1^\bullet(t)u_1(t) + M_2^\bullet(t)u_2(t) + M_3^\bullet(t)u_3(t)\right]$$

$$-\frac{k_i}{2}\left[2R_0^\bullet(t)u_0(t) + R_1^\bullet(t)u_1(t) + R_2^\bullet(t)u_2(t) + R_3^\bullet(t)u_3(t)\right]$$

$$-\frac{k_{ri}}{2}\left[2RI_0^\bullet(t)u_0(t) + RI_1^\bullet(t)u_1(t) + RI_2^\bullet(t)u_2(t) + RI_3^\bullet(t)u_3(t)\right],$$

$$(34a)$$

$$\frac{du_1(t)}{dt} = -\frac{S_1 k_p}{2}\Big[2M_1^\bullet(t)u_0(t) + 2M_0^\bullet(t)u_1(t) + M_2^\bullet(t)u_1(t) + M_1^\bullet(t)u_2(t)$$

$$+ M_3^\bullet(t)u_2(t) + M_2^\bullet(t)u_3(t)\Big] - \frac{k_i}{2}\Big[2R_1^\bullet(t)u_0(t) + 2R_0^\bullet(t)u_1(t)$$

$$+ R_2^\bullet(t)u_1(t) + R_1^\bullet(t)u_2(t) + R_3^\bullet(t)u_2(t) + R_2^\bullet(t)u_3(t)\Big]$$

$$-\frac{k_{ri}}{2}\Big[2RI_1^\bullet(t)u_0(t) + 2RI_0^\bullet(t)u_1(t) + RI_2^\bullet(t)u_1(t) + RI_1^\bullet(t)u_2(t)$$

$$+ RI_3^\bullet(t)u_2(t) + RI_2^\bullet(t)u_3(t)\Big] - K^2\Bigg\{\Big[D_{m,0}(t) - \frac{1}{2}D_{m,2}(t)\Big]u_1(t)$$

$$+ \Big[D_{m,1}(t) - D_{m,3}(t)\Big]u_2(t) - \frac{3}{2}D_{m,2}(t)u_3(t)\Bigg\},$$

(34b)

where $S_l = \exp\big(-l^2 K^2 \sigma/2\big)$ [30-32,50]. For generality, in Eq. (34b), we retain $D_{m,0}$, $D_{m,1}$, $D_{m,2}$ and $D_{m,3}$. However, in our simulations, we assume $D_{m,j>0} = 0$ [30-32,50].

These coupled equations along with those presented in Section 3 are then solved under the initial conditions,

$$D_0(t=0) = D_0,\ CI_0(t=0) = CI_0,\ u_0(t=0) = U_0,\ CTA_0(t=0) = CTA_0, Z_0(t=0) = Z_0,$$

$$D_{n>0}(t=0) = CI_{n>0}(t=0) = u_{n>0}(t=0) = CTA_{n>0}(t=0) = Z_{n>0}(t=0) = 0,\ \text{and}$$

$$D_{n\geq0}^*(t=0) = HD_{n\geq0}^\bullet(t=0) = R_{n\geq0}^\bullet(t=0) = RI_{n\geq0}^\bullet(t=0) = M_{n\geq0}^\bullet(t=0) = N_{n\geq0}(t=0) = 0.$$

(35)

4.3 Numerical Results

We will now examine some of the predictions of the extended model presented in this section. Unless otherwise stated all kinetic parameter values are assigned appropriate values, which are typical for the AA/PVA photopolymer material examined. The simulations are performed retaining four spatial concentration harmonics and the coupled differential equations are solved using the initial conditions given in Eq. (35). In all cases, $U_0 = 2.83\times10^{-3}$ mol/cm^3, $D_0 = 1.22\times10^{-6}$ mol/cm^3, $ED_0 = 3.18\times10^{-3}$ mol/cm^3, $CTA_0 = 1\times10^{-6}$ mol/cm^3, and $Z_0 = 1\times10^{-8}$ mol/cm^3 [30-34], where U_0, D_0, ED_0, CTA_0 and Z_0 represent the concentrations of monomer, photosensitizer, electron donor, transfer agent and inhibitor, respectively. We also assume that all time varying viscosity effects are negligible, i.e., $D_{m,j>0} = 0$, and that, $D_{m0} = 1.0\times10^{-10}$ cm^2/s. The exposure intensity chosen is $I_0 = 1$ mW/cm^2, the recording wavelength is $\lambda = 532$ nm and the layer thickness $d = 100$ μm. The absorption parameters are, $\varepsilon = 1.43\times10^8$ cm^2/mol, $\phi = 0.01$ mol/Einstein and $T_{sf} = 0.76$. The oxygen diffusion coefficient is $D_z(x,t) = D_z = 1.0\times10^{-8}$ cm^2/s and $\tau_z = 0$, i.e., sealed layers are used [32]. The typical rate constants used were: $k_p = k_i = 1\times10^7$ cm^3/mol s, $k_t = 3\times10^8$ cm^3/mol s, $k_{tp} = k_t \times 10$, $k_d = k_b = 1.6\times10^3$ cm^3/mol s, $k_{tr} = 1\times10^7$ cm^3/mol s, $k_{ri} = 1\times10^6$ cm^3/mol s, $k_z = 3\times10^{12}$ cm^3/mol s, and $k_r = 1.2\times10^{-3}$ s^{-1} [30-34,48]. Assuming typical recording conditions for an unslanted transmission type volume holographic grating, i.e., period $\Lambda = 400$ nm and fringe visibility $V = 1$, the resulting predictions of the temporal and spatial behaviour of the photochemical processes are now examined.

As different types of chain transfer agents will exhibit different kinetic behaviours, which result in variations in the polymerization rate and therefore changes to the number-average degree of polymerization, DP_n [48]. The results presented in Figure 9 demonstrate the effects of varying the initial CTA concentration on the DP_n when the re-initiation rate $k_{ri} = 1\times10^6$ cm^3/mol s. For a particular type of CTA, i.e., when $k_{tr} = 1\times10^7$ cm^3/mol s, it can be seen that increasing the initial CTA concentration leads to a rapid decrease in DP_n and that the value for DP_n decreases more slowly to lowest value shown. This result indicates that, for an appropriate concentration of CTA, i.e., $1\times10^{-6} < CTA_0 < 4\times10^{-6}$ mol/cm^3, DP_n is always reduced with the inclusion of CTA and that the reduction is larger for higher CTA concentrations. Furthermore, when $k_{tr} \geq 1\times10^7$ cm^3/mol s, the model predicts that above some specific CTA concentration a threshold exists and further increases do not result in any further significant reduction in DP_n, i.e., when $CTA_0 > 4\times10^{-6}$ mol/cm^3. Ideally, one wishes to identify the least amount of CTA required in order to achieve the largest reduction in the number-average of polymerization, DP_n. We also note that, for the same initial CTA concentration, a reduction in DP_n also takes place for an increase in chain transfer kinetic value, k_{tr}. Thus the addition of different types and concentrations of chain transfer agents are predicted to have different effects on the value of DP_n and therefore on the average polymer chain length in the otherwise identical photopolymer system. As discussed in earlier the non-local response length, $\sqrt{\sigma}$, and the number-average degree of polymerization, DP_n, are both related to the average polymer chain length. We would expect that any significant reduction in the number-average degree of polymerization, DP_n, should be accompanied by a reduction in the non-local response length, $\sqrt{\sigma}$, and therefore by an improvement in the refractive index modulation, n_1, which can be recorded at high spatial frequencies in the material.
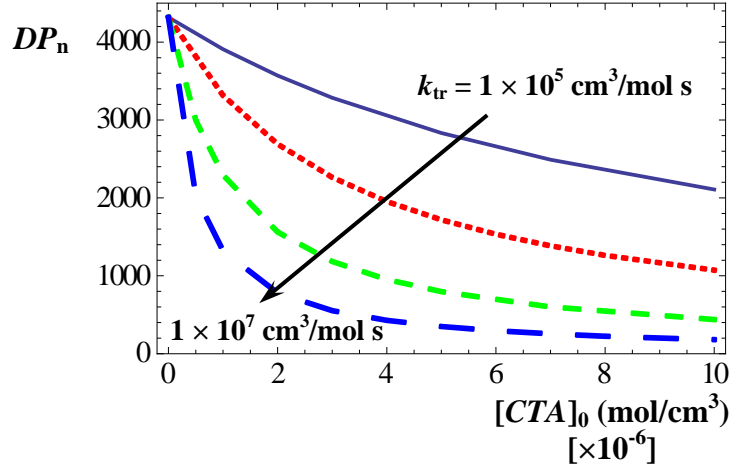
Figure 9. Effects of initial CTA concentration on number-average degree of polymerization, DP_n, and contributions of various rate constants of chain transfer, k_{tr}, [cm³/mol s]: {1×10^5 (solid); 3×10^5 (short dashed); 1×10^6 (dashed) and 1×10^7 (long dashed)}.

In order to demonstrate the relationship between the non-local response length, $\sqrt{\sigma}$, and the refractive index modulation, n_1, Figure 10 shows four simulated growth curves of refractive index modulation, n_1, for four different values of $\sqrt{\sigma}$. In all cases the same rate constant values that were used above are employed. We see that larger values of $\sqrt{\sigma}$, lead to lower saturation (maximum) values of n_1 for the same grating period. In another words, the lower the value of $\sqrt{\sigma}$ the more localized the polymerization process and hence the shorter the polymer chains grown during holographic grating formation.
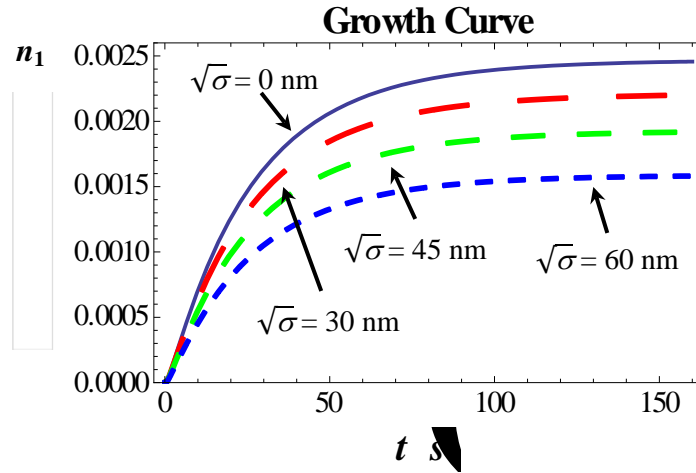

Figure 10. Simulations of the growth curves of refractive index modulation, n_1, at $\Lambda = 400$ nm for various values of non-local response length, $\sqrt{\sigma}$ nm: {0 nm (solid); 30 nm (long dashed); 45 nm (dashed) and 60 nm (short dashed)}.

Figure 11 shows the saturation refractive index modulation, n_1^{sat}, plotted as a function of the grating spatial frequency, for the same grating parameter values, as those used in the generation of Figure 10. These results predict that lower $\sqrt{\sigma}$ values lead to a significant improvement in the high spatial frequency response of the material and therefore a reduction in the high spatial frequency roll-off observed experimentally. This is an important prediction of the NPDD model and motivates the study of the feasibility of applying chain transfer agents in free radical based photopolymer materials.
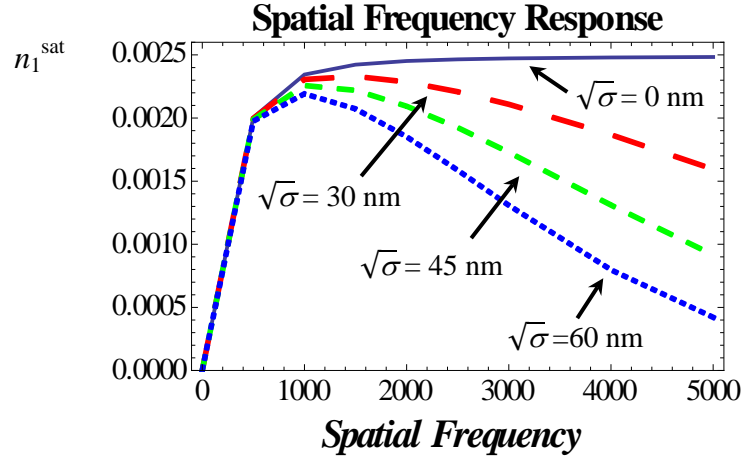
Figure 11. Simulations of the spatial frequency response of the refractive index modulation at saturation, n_1^{sat} for various values of the non-local response length, $\sqrt{\sigma}$ nm: {0 nm (solid); 30 nm (long dashed); 45 nm (dashed) and 60 nm (short dashed)}.

4.4 Experimental Results

In this subsection, we aim to demonstrate and compare the effects of a number of CTAs on the spatial frequency response of the various photopolymer material compositions under examination. Following the analysis presented in Section 4.3, we aim to show that a reduction in average polymer chain length results in the predicted reduction in the non-local chain length $\sqrt{\sigma}$ and hence an increase in the material's response at high spatial frequencies. In order to achieve this, experimentally obtained growth curves and the saturation values of refractive index modulation, n_1^{sat}, for three photopolymer material compositions, over a range of spatial frequencies from 500 to 4799 lines/mm, are measured and compared [29,33,34].

The three material compositions examined are; (i) a standard acrylamide/polyvinylalcohol photopolymer [30-34], (ii) the standard acrylamide/polyvinylalcohol photopolymer with the addition of 0.96 g of sodium formate (CTA-1) [29,32,32] and (iii) the standard acrylamide/polyvinylalcohol photopolymer with 0.53 ml of 1-mercapto-2-propanol (CTA-2). .For each sample of these material composition examined, several growth curves were measured using a recording intensity of 1 mW/cm², at a recording wavelength of $\lambda = 532$ nm, in order to ensure experimental reproducibility. In all cases the diffraction efficiency of a probe beam, at $\lambda_p = 633$ nm was monitored during and post-exposure and angular scans of the gratings performed and analysed.

Applying the extended NPDD model presented in the previous subseciton, the experimental growth curve data was fit using a least squares algorithm, in which the Mean Square Error (MSE) between the prediction of the model and the experimental data was minimized to extract key material parameters. In order to carry out the fitting process, search ranges of typical parameter values based on data presented in the literature were used [30-34,48]. The model was then applied to analyse the temporal variation of the refractive index modulation n_1, for each of the materials at over the range of spatial frequencies examined. In this way the monomer diffusion constant D_{m0}, the propagation rate constant, k_p, the initial rate, k_i, bimolecular termination rate constant, k_t, the primary termination rate, k_{tp}, the chain transfer rate, k_{tr}, the re-initiation rate, k_{ri}, and the non-local response length, $\sqrt{\sigma}$, were all estimated.

The parameters estimated for the compositions studied are presented in Table 3 (standard AA/PVA), Table 4 (CTA-1) and Table 5 (CTA-2). For each spatial frequency the saturation refractive index modulation value, n_1^{sat} , is provided in the first column of each table.

Examining the estimated values for k_p, k_t and D_{m0} given in three tables, it can be seen that they are consistent and close to the values previously reported in the literature [30-34,48]. In particular we note that the mean values estimated for D_{m0}, given in all the tables, are very similar [30-34]. The values obtained for the parameters, k_{tr} and k_{ri}, in Table 4 and 5, lie within reasonable ranges based on the values reported in the literature [48]. They clearly indicate the different physical properties of the two CTAs when used in an AA/PVA based photopolymer material. For each CTA being examined, it should also be noted that the values found for k_{tr} and k_{ri}, are consistent for each of the different spatial frequencies.

SF (lines/mm) [$n_1^{\text{sat}} \times 10^{-3}$]	k_p (×10^7)	k_t (×10^8)	D_{m0} (×10^-10)	$\sqrt{\sigma}$ (nm)	MSE (×10^-10)
500 [2.07]	2.7	3.0	3.0	60	1.96
1000 [2.20]	2.3	3.6	1.0	68	1.64
1428 [2.36]	2.8	3.0	3.0	55	0.89
2000 [1.97]	2.2	3.8	2.0	60	1.09
2500 [1.56]	2.7	3.1	3.0	65	1.21
3000 [1.38]	2.6	3.2	3.0	60	2.72
Mean	**2.6±0.4**	**3.3±0.5**	**2.5±1.5**	**61.3±6.7**	**1.59±1.13**

Table 3: Spatial frequency parameter estimations for standard AA/PVA material.

SF (lines/mm) [$n_1^{\text{sat}} \times 10^{-3}$]	k_p (×10^7)	k_t (×10^8)	D_{m0} (×10^-10)	k_{tr} (×10^6)	k_{ri} (×10^7)	$\sqrt{\sigma}$ (nm)	MSE (×10^-10)
500 [1.90]	3.7	3.3	5.0	5.0	2.6	50	1.64
1000 [2.18]	3.5	3.4	3.0	2.0	1.0	51	2.72
1428 [2.39]	3.8	3.0	6.0	3.0	1.3	45	2.65
2000 [2.12]	3.2	4.0	6.0	2.0	1.7	45	2.36
2500 [1.87]	3.7	3.0	3.0	3.0	1.0	49	3.92
3000 [1.60]	3.8	3.6	1.0	2.0	1.0	47	1.17
Mean	**3.6±0.4**	**3.4±0.6**	**4.0±3.0**	**2.8±2.2**	**1.4±1.2**	**47.6±3.4**	**2.41±1.24**

Table 4: Parameter estimations for spatial frequencies in AA/PVA with sodium formate (CTA-1) material.

SF (lines/mm) [$n_1^{\text{sat}} \times 10^{-3}$]	k_p (×10^7)	k_t (×10^8)	D_{m0} (×10^-10)	k_{tr} (×10^7)	k_{ri} (×10^6)	$\sqrt{\sigma}$ (nm)	MSE (×10^-10)
500 [1.97]	2.0	3.5	5.0	1.0	8.0	40	1.98
1000 [2.09]	1.7	3.8	3.0	2.0	6.0	40	1.71
1428 [2.38]	1.6	3.9	2.0	2.0	3.0	42	1.53
2000 [2.23]	1.7	3.7	6.0	3.0	2.0	40	1.22
2500 [2.03]	2.1	3.0	2.0	1.0	3.0	38	5.53
3000 [1.68]	1.7	3.8	2.0	1.0	8.0	39	1.12
Mean	**1.8±0.3**	**3.6±0.6**	**3.3±2.7**	**1.7±1.3**	**5.0±3.0**	**39.8±2.2**	**2.18±3.35**

Table 5: Parameter estimations for spatial frequencies in AA/PVA with 1-mercapto-2-propanol (CTA-2) material.

In Table 3 the mean non-local response length in the standard AA/PVA material is estimated to be approximately $\sqrt{\sigma} \approx 61.3$ nm. This value agrees well with the previous estimates reported in the literature [29-34]. For the material containing sodium formate (CTA-1), the corresponding value is $\sqrt{\sigma} \approx 47.6$ nm, as given in Table 4, which corresponds to a reduction ~22.3% in the mean non-local response length, $\sqrt{\sigma}$. In Table 5, the $\sqrt{\sigma}$ value obtained for the material with 1-mercapto-2-propanol (CTA-2) is $\sqrt{\sigma} \approx$

39.8 nm. This corresponds to a ~35.0%, reduction in the mean $\sqrt{\sigma}$ value. Therefore significant improvements in the high spatial frequency responses with the addition of CTA can be clearly observed. CTA-2 is more effective in reducing the average polymer chain length. Furthermore, in very high spatial frequencies, the results consistently indicate an accompanying improvement in the magnitude of the saturation refractive index modulation. Based on the analysis above it is clear that shortening the polymer chains through the addition of chain transfer agents improves this photopolymer's spatial frequency response.

In order to more clearly illustrate the results presented in Tables 3 - 5 the spatial frequency response of each material are shown in Figure 12.
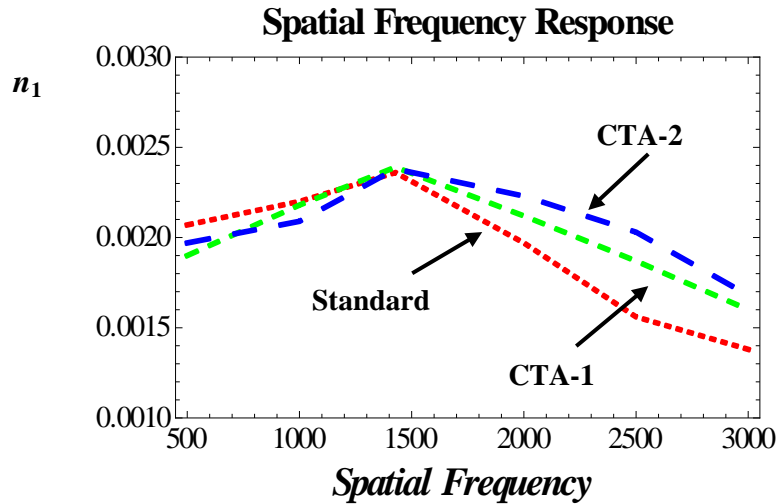

Figure 12. Experimental results of spatial frequency response of saturation refractive index modulation, n_1, variation, for standard material (small dashed line), standard material with 0.96g sodium formate (CTA-1) (medium dashed line) and standard material with 0.53ml 1-mercapto-2-propanol (CTA-2) (large dashed line).

The improvements in the high spatial frequency response can clearly be observed. In order to demonstrate the improvements in AA/PVA material performance, numerical fits were carried out to the growth curves of all the three testing samples, for the 3000 lines/mm spatial frequency case. The results are presented in Figure 13 with the associated error bars, indicating the reproducibility of the experimental results.
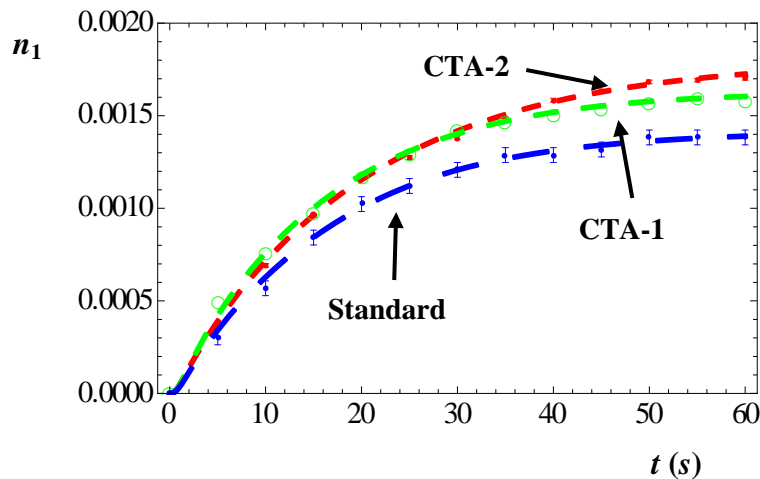

Figure 13. Experimental growth curve data with error bars and fits at 3000 lines/mm, standard material (large dashed line); with sodium formate, CTA-1, (medium dashed line and empty circle points) and with 1-mercapto-2-propanol, CTA-2, (small dashed line).

In this section the NPDD model was extended to examine the effects of the addition of CTAs to an AA/PVA photopolymer. As the NPDD model predicts, a reduction in average polymer chain length grown during polymerisation will reduce the negative smearing effects which are caused by non-local polymer chain growth. As CTAs are known to reduce the average polymer chain length grown during polymerisation, a number of various types and concentrations of CTA were added to reduce these detrimental effects. Then using the NPDD model and fitting growth curves of refractive index modulation at various spatial frequencies for each of the compositions under examination, estimates of key material parameters were obtained. All results verified that the use of CTAs caused a substantial increase in the response of the AA/PVA photopolymer's spatial frequency response, particularly at higher spatial frequencies, which is in line with the NPDD model predictions.

5.   CONCLUSION

In this chapter we briefly reviewed some of the developments made in the area of photopolymer material development. We also examined some of the extensions which have been made to the Non-local Photo-polymerisation Driven Diffusion (NPDD) model in order to increase its physicality, with the aim of producing a tool for photopolymer material optimization. A detailed understanding of the photochemical and photo-physical effects which take place during and after holographic exposure is of extreme importance in order to achieve such a tool. Some of the recent developments which have been made in order to achieve this were illustrated and their implications examined. Among these were the temporal and spatial primary radical, the effects of oxygen inhibition, non-local polymer chain growth and the addition of chain transfer agents to improve the spatial frequency response. As various photopolymer compositions have diverse chemical and structural characteristics, knowledge of the characteristics required when choosing these components will offer an informed choice to yield specific improvements in material performance. The implications of the predictions presented here suggest that there are many ways in which improvements can be made.

There still remain a number of effects which have not been included into the NPDD model which would increase its physicality and therefore make it a more powerful tool. One of these which has not been included here, is the addition of time varying viscosity effects. When polymerisation occurs, densification and crosslinking occurs, resulting in a reduction in the material's fractional free volume. This reduction causes an increase in the viscosity of the material which restricts the rate at which polymerisation proceeds. Accurate modelling of these effects would allow for more precise recording schedules for subsequent holographic exposures to be determined and would enable optimum concentration ratios of the main constituents of the material to be found. T

REFERENCES

[1]   Close D H, Jacobson A D, Magerum R C, Brault R G, McClung F J (1969), Hologram recording on photopolymer materials. Appl. Phys. Lett. j. 14: 159-160.

[2]   InPhase Technologies (2007), www.inphase-technologies.com Tapestry Media.

[3]   Maruo S, Nakamura O, Kawata S (1997), Three-dimensional microfabrication with two-photon-absorbed photopolymerization. Opt. Lett. j. 22: 132-134.

[4]   Saravanamuttu K, Blanford C F, Sharp D N, Dedman E R, Turberfield A J, Denning R G (2003) Sol-gel organic-inorganic composites for 3-D holographic lithography of photonic crystals with submicron periodicity. Chem. Mater. j. 15: 2301-2304.

[5]   Gu M, Straub M, Nguyen L H, (2004), Complex-shaped 3-D microstructures and photonic crystals generated in a polysiloxane polymer by two-photon microstereolithography. Opt. Mater. j. 27: 359-364.

[6]   Sullivan A C, Grabowski M W, McLeod R R, (2007), Three-dimensional direct-write lithography into photopolymer. Appl. Opt. j. 46: 295-301.

[7]   Dhar L, Hale A, Katz H E, Schilling M L, Schnoes M G, Schilling F C (1999), Recording media that exhibit high dynamic range for digital holographic data storage. Opt. Lett. j. 24: 487-489.

[8]   Dhar L, Hale A, Kurtis K, Schnoes M, Tackitt M, Wislon W, Hill A, Schilling M, Katz H, Olsen A (2000), Photopolymer recording media for high density data storage. IEEE Conf. Digest: Optical Data Storage 158-160.

[9]   Schultz S, Glytsis E, Gaylord T (2000), Design, fabrication, and performance of preferential-order volume grating waveguide couplers. Appl. Opt. j. 39: 1223-1232.

[10]   Sato A, Scepanovic M, Kostuk R (2003), Holographic edge-illuminated polymer bragg gratings for dense wavelength division optical filters at 1550 nm. Appl. Opt. j. 42: 778-784.

[11]   Sheridan J T, Kelly J V, O'Brien G, Gleeson M R, O'Neill F T (2004), Generalized non-local responses and higher harmonic retention in non-local polymerization driven diffusion model based simulations. J. Opt. A: Pure Appl. Opt. j. 6: 1089-1096.

[12]   McLeod R R, Daiber A J, McDonald M E, Robertson T L, Slagle T, Sochava S L, Hesselink L (2005), Microholographic multilayer optical disk data storage. Appl. Opt. j. 44: 3197-3207.

[13]   Milster T D (2005), Horizons for optical storage. Opt. Photon. News. j. 16: 28-33.

[14]   Barachevskii V A (2006), Photopolymerizable recording media for three-dimensional holographic optical memory. High Energy Chem. j. 40: 131-141.

[15]   Sheridan J T, Gleeson M R, Kelly J V, Close C E, O'Neill F T (2006), Optimized holographic data storage: diffusion and randomization. J. Opt. A: Pure Appl. Opt. j. 8: 236-243.

[16]   Toisihi M, Tanaka R, Watanabe K, Betsuyaku K (2007), Analysis of photopolymer media of holographic data storage using non-local polymerization driven diffusion model. Jap. J. Appl. Phys. j. 46: 3438-3447.

[17]   Nagy Z, Koppa P, Ujhelyi F, Dietz E, Frohmann S, Orlic S (2007), Modelling material saturation effects in microholographic recording. Opt. Exp. j. 15: 1732-1737.

[18]   Toishi M, Takeda T, Tanaka K, Tanaka T. Fukumoto A, Watanabe K (2008), Two-dimensional simulation of holographic data storage medium for multiplexed recording. Opt. Exp. j. 16: 2829-2839.

[19]   Sadlej N, Smolinska B (1975), Stable photo-sensitive polymer layers for holography. Opt. Laser Technol. j. 7: 175-179.

[20]   Calixto S (1987), Dry polymer for holographic recording. Appl. Opt. j. 26: 3904-3909.

[21]   Blaya S, Mallavia R, Carretero L, Fimia A, Madrigal R F (1998), Highly sensitive photopolymerisable dry film for use in real time holography. Appl. Hys. Lett. j. 75: 1628-1630.

[22]   Zhao F, Frietmann E E, Li X (1998), Novel type of red sensitive photopolymer system for optical storage. Proc. SPIE. j. 3486: 317-321.

[23]   Trentler T, Boyd J, Colvin V (2000), Epoxy resin photopolymer composites for volume holography. Chem. Mater. j. 12: 1431-1438.

[24]   Bayer MaterialScience AG, www.bayermaterialscience.com.

[25]   Rolle T, Bruder F-K, Facke T, Weiser M-S, Honel D, Stoeckel N (2010), (2010), "Photopolymerzusammensetzungen für optische Elemente und visuelle Darstellungen. EP2 172 505 A1.

[26]   Gleeson M R, Sheridan J T, Bruder F-K, Roelle T, Honnell D, Weiser M-S, Faecke T (2011), Comparison of a new self-developing photopolymer with AA/PVA based photopolymer utilizing the NPDD model. Opt. Exp. j. 19: 26325-26342.

[27]   Gleeson M R, Guo J, Sheridan J T (2011), Optimisation of Photopolymers for Holographic Applications using the Non-Local Photo-Polymerization Driven Diffusion Model. Opt. Exp. j. 19: 22423-22436.

[28]   Gleeson M R, Kelly J V, Sabol D, Close C E, Liu S, Sheridan J T (2007), Modelling the photochemical effects present during holographic grating formation in photopolymer materials. J. Appl. Phys. j. 102: 023108.

[29]   Gleeson M R, Sabol D, Liu S, Close C E, Kelly JV, Sheridan J T (2008), Improvement of the spatial frequency response of photopolymer materials by modifying polymer chain length. J. Opt. Soc. Am. B. j. 25: 396-406.

[30]   Gleeson M R, Sheridan J T (2009), Non-local photo-polymerization kinetics including multiple termination mechanisms and dark reactions: Part I. Modelling. J. Opt. Soc. Am. B. j. 26: 1736-1745.

[31]   Gleeson M R, Liu S, McLeod R R, Sheridan T (2009), Non-local photo-polymerization kinetics including multiple termination mechanisms and dark reactions: Part II. Experimental Validation. J. Opt. Soc. Am. B. j. 26: 1746-1754.

[32]   Gleeson M R, Liu S, Guo J, Sheridan J T (2010), Non-local photo-polymerization kinetics including multiple termination mechanisms and dark reactions: Part III. Primary radical generation and inhibition. J. Opt. Soc. Am. B. j. 27: 1804-1812.

[33]   Guo J, Gleeson M R, Liu S, Sheridan J T (2011), Non-Local Spatial Frequency Response of Photopolymer materials containing Chain Transfer Agents: Part I. Theoretical Model. J. Opt. A: Pure Appl. Opt. j. 13: 095601.

[34]   Guo J, Gleeson M R, Liu S, Sheridan J T (2011), Non-Local Spatial Frequency Response of Photopolymer materials containing Chain Transfer Agents: Part II. Experimental Results. J. Opt. A: Pure Appl. Opt. j. 13: 095602.

[35]   Kogelnik H (1969), Coupled wave theory for thick hologram gratings. Bell Syst. Tech. J. j.48: 2909-2945.

[36]   Syms R R A (1990), Practical Volume Holography, In Clarendon Press, Oxford.

[37]   O'Neill F T, Lawrence J R, Sheridan J T (2000), Automated recording and testing of holographic optical element arrays. Optik. j. 111: 459-467.

[38]   Fimia A, Lopez N, Mateos F, Sastre R, Pineda J, Amatguerri F (1993), Elimination of oxygen inhibition in photopolymer system used as holographic recording materials. J. Mod. Opt. j. 40: 699-706.

[39]   Manivannan G, Lessard R A (1994), Trends in holographic recording materials. Trends Polym. Sci. j. 2: 282-290.

[39]   Lawrence J R, O'Neill F T, Sheridan J T (2001), Photopolymer holographic recording material. Optik j. 112: 449-463.

[40]   O'Brien A K, Bowman C N (2006), Modeling the effect of oxygen on photopolymerization kinetics. Macromol. Theor. Sim. j. 15: 176-182.

[41]   Harbour S, Kelly J V, Galstian T, Sheridan J T (2007), Optical birefringence and anisotropic scattering in acrylate based holographic polymer dispersed liquid crystals. Opt. Comm. j. 278: 28-33.

[42]   Bowman C N, Peppas N A (1991), Coupling of kinetics and volume relaxation during polymerizations of multiacrylates and multimethacrylates. Macromol. j. 28: 1914-1920.

[43].   Aubrecht I, Miller M, Koudela I (1998), Recording of holographic diffraction gratings in photopolymers: Theoretical modelling and real-time monitoring of grating growth. J. Mod. Opt. j. 45: 1465-1477.

[44]   Gleeson M R, Sheridan J T (2009), A review of the modelling of free-radical photopolymerisation in the formation of holographic gratings. J. Opt. A: Pure Appl. Opt.: Special Issue, Optics of Nanocomposite Materials. j. 10: 024008.

[45]   Carretero L, Blaya S, Mallavia R, Madrigal R F, Belendez A, Fimia A (1998), Theoretical and experimental study of the bleaching of a dye in a film-polymerization process. Appl. Opt. j. 37: 4496-4499.

[46]   Gleeson M R, Liu S, O'Duil S, Sheridan J T (2008), Examination of the photoinitiation processes in photopolymer materials. J. Appl. Phys. j. 104: 064917.

[47]   Gallego S, Ortuno M, Neipp C, Marquez A, Belendez A, Pascual I, Kelly J V, Sheridan T (2005), Physical and effective optical thickness of holographic diffraction gratings recorded in photopolymers. Opt. Exp. j. 13: 1939-1947.

[48]   Odian G (1991), Principles of Polymerization. Wiley New York.

[49]   Gleeson M R, Kelly J V, Close C E, O'Neill F T, Sheridan J T (2006), Effects of absorption and inhibition during grating formation in photopolymer materials. J. Opt Soc. Am. B. j. 23: 2079-2088.

[50]   Sheridan J T, Lawrence J R (2000), Nonlocal response diffusion model of holographic recording in photopolymer. J. Opt. Soc. Am. A. j. 17: 1108-1114.

[51]   Crank J (1956), The Mathematics of Diffusion. Oxford University Press.

[52]   Mayo F R (1943), Chain Transfer in the Polymerization of Styrene: The Reaction of Solvents with Free Radicals. J. Am. Chem. Soc. j. 65: 2324-2329.

[53]   Goretta L A, Otremba R R (1981), U.S. Patent No. 4,307,215.

[54]   Gartner H A (1992), U.S. Patent No. 5,171,783.

[55]   Fevola M, Hester R, McCormack C (2003), Molecular weight control of Polyacyrlamide with Sodium Formate as a Chain-Transfer Agent: Characterization via size Exclusion Chromatography/multi-angle laser light scattering and determination of chain-Transfer constant. J. Polym. Sci., Part A: Poly. Chem. j. 41: 560-568.

[56]   Valdebenito A, Encinas M V (2005), Thiophenols as chain transfer agents in the polymerization of vinyl monomers. Polymer. j. 46: 10658-10662.

[57]   Okaya T, Kikuchi K, Morii Y (1997), Polymerization of acrylamide in aqueous medium initiated with a redox system composed of cysteine and potassium bromate. Macromol. Chem. Phys. j. 198: 2027-2034.